AGU PUBLICATIONS

Water Resources Research

RESEARCH ARTICLE
10.1002/2014WR015692

Key Points:
- Framework for the seasonal water balance is developed based on climatic controls
- The 321 catchments are grouped into 10 clusters with similar seasonal water balances
- The seasonal water balance has an imprint both on streamflow and landscape

Correspondence to:
W. R. Berghuijs,
wb14708@bristol.ac.uk

Citation:
Berghuijs, W. R., M. Sivapalan, R. A. Woods, and H. H. G. Savenije (2014), Patterns of similarity of seasonal water balances: A window into streamflow variability over a range of time scales, *Water Resour. Res.*, *50*, 5638–5661, doi:10.1002/2014WR015692.

Received 9 APR 2014
Accepted 23 JUN 2014
Accepted article online 26 JUN 2014
Published online 9 JUL 2014

Patterns of similarity of seasonal water balances: A window into streamflow variability over a range of time scales

Wouter R. Berghuijs[1,2], Murugesu Sivapalan[3], Ross A. Woods[2], and Hubert H. G. Savenije[1]

[1]Water Resources Section, Delft University of Technology, Delft, Netherlands, [2]Department of Civil Engineering, University of Bristol, Bristol, UK, [3]Department of Geography and Geographic Information Science and Department of Civil and Environmental Engineering, University of Illinois at Urbana-Champaign, Urbana, Illinois, USA

Abstract Recent hydrologic synthesis efforts have presented evidence that the seasonal water balance is at the core of overall catchment responses, and understanding it will assist in predicting signatures of streamflow variability at other time scales, including interannual variability, the flow duration curve, low flows, and floods. In this study, we group 321 catchments located across the continental U.S. into several clusters with similar seasonal water balance behavior. We then delineate the boundaries between these clusters on the basis of a similarity framework based on three hydroclimatic indices that represent aridity, precipitation timing, and snowiness. The clustering of catchments based on the seasonal water balance has a strong relationship not only with regional patterns of the three climate indices but also with regional ecosystem, soil, and vegetation classes, which point to the strong dependence of these physiographic characteristics on seasonal climate variations and the hydrologic regimes. Building on these catchment clusters, we demonstrate that the seasonal water balance does have an imprint on signatures of streamflow variability over a wide range of time scales (daily to decadal) and a wide range of states (low flows to floods). The seasonal water balance is well integrated into variability at seasonal and longer time scales, but is only partly reflected in the signatures at shorter time scales, including flooding responses. Overall, the seasonal water balance has proven to be a similarity measure that serves as a link between both short-term hydrologic responses and long-term adaptation of the landscape with climate.

1. Introduction

The well-known heterogeneity and complexity associated with catchments make it difficult to produce generalizations of their streamflow response beyond individual catchments [*Dooge*, 1986; *Beven*, 2000; *McDonnell et al*., 2007]. Yet, despite the heterogeneity and complexity present in individual catchments, it is generally believed that they hold some level of internal organization and simplicity of responses, which should permit a degree of predictability of their functional behavior [*Dooge*, 1986; *Savenije*, 2001; *Sivapalan*, 2003; *McDonnell et al*., 2007]. One example of generalized predictive behavior is that the mean-annual partitioning of precipitation into evaporation and streamflow is primarily a function of the relative atmospheric supply and demand of water, expressed by the aridity index, the ratio of the mean available energy (potential evaporation) to mean available water (precipitation) at the annual scale [*Pike*, 1964; *Budyko*, 1974]. This understanding of the process control of the annual water balance would allow a priori prediction, albeit to first order, of long-term average streamflows for catchments where no streamflow measurements are available [*McMahon et al*., 2013]. It has been shown that the energy versus water competition, as per the Budyko hypothesis, can even extend to the interannual variability of the annual water balance [*Milly and Dunne*, 2002; A. D. Carmona et al., Regional patterns of inter-annual variability of catchment water balances across the continental United States: Separating the roles of climatic and bio-geophysical controls, submitted to *Water Resources* Research, 2014]. Additionally, it would provide a framework for catchment intercomparisons [*Falkenmark and Chapman*, 1989], for uncovering additional secondary controls, and for studying changes to the long-term water balance of catchments in response to climate and land cover change [e.g., *Dooge*, 1992; *Zhang et al*., 2001; *Gerrits et al*., 2009; *Li et al*., 2013].

The dominant climatic and landscape controls on hydrologic responses are time scale dependent [*Atkinson et al*., 2002; *Farmer et al*., 2003]. Therefore, a natural extension of the Budyko-type framework would be one that might help to understand the physical controls on the similarity and differences of streamflow variability at shorter time scales. In this paper, we focus on developing a similarity framework for seasonal water

balance behavior and the imprint of such seasonal water balance on signatures of streamflow variability at a range of other time scales. In the past, similarity metrics to group catchments with similar seasonal water balance behavior have been based on streamflow characteristics themselves [*Pardé*, 1933; *Haines et al*., 1988; *Weingartner and Aschwanden*, 1992; *Hannah et al*., 2005; *Petersen et al*., 2012], climate characteristics [*Köppen*, 1936; *Peel et al*., 2007], catchment characteristics [*Breinlinger*, 1996; *Laizé and Hannah*, 2010], hybrids of both climate and catchment characteristics [*Woods*, 2003; *Yokoo et al*., 2008], and combinations of streamflow and climate characteristics [*Coopersmith et al*., 2012]. In this paper, we extend the similarity analysis beyond streamflow variability alone, and to explicitly include the fullness of the seasonal water balance.

Classification studies based on observed streamflow data alone help us to cluster catchments together on the basis of their similarity and even produce regional maps, but without explicit consideration of the underlying process controls (be they climate or landscape factors) they are unable to be used to make predictions in ungauged basins across noncontiguous regions. While spatial proximity can be used as a surrogate for catchment similarity [*Andréassian et al*., 2012] under some circumstances, ideally, a similarity framework should be process based, and yet provide a foundation for comparative studies aimed at learning from observed data [*Wagener et al*., 2007]. The key process that underpins seasonal streamflow behavior is the storage variation that results in response to timing differences between water availability (rainfall plus snowmelt) and energy availability (potential evaporation) [*Wundt*, 1953; *Thornthwaite and Mather*, 1955; *Willmott et al*., 1985].

The development of a similarity framework for the comparative analysis of the seasonal water balance would be of particular interest as these seasonal variations impact streamflow variability not just seasonally, but at other time scales as well. For example, in cold regions, accumulation during winter and subsequent melting of the snowpack and ice during spring produce strong seasonal streamflow variations. Because the seasonal water balance impacts the variations of soil moisture or snow storage and more generally, antecedent wetness conditions, it can have a major impact on runoff variability at event scales, and in this way affect streamflow variability at all time scales and states [*Blöschl et al*., 2013]. At shorter time scales, for example, the seasonal water balance has been shown to control the middle part of the flow duration curve and thereby forms the connection between high flows and low flows [*Yokoo and Sivapalan*, 2011; *Yaeger et al*., 2012; *Ye et al*., 2012]. Over longer time scales, the seasonal water balance leaves an imprint not only on the annual water balance and interannual variability, but is also reflected in the vegetation types that become established [*Stephenson*, 1990], and more generally, in ecosystem productivity [*Harris et al*., 2000; *Robinson et al*., 2012]. Consequently, the seasonal water balance behavior may provide ecohydrological insights into regional patterns of climate-soil-vegetation dynamics and help to delineate regions with fundamentally different hydrologic regimes [*Rodriguez-Iturbe*, 2000].

The aim of this paper is to develop a similarity framework to characterize seasonal water balance behavior, specifically including storage variations as well as the more general seasonal streamflow variations. The development of such a similarity framework, and the testing of hypotheses regarding the central role of the seasonal water balance in streamflow variability at all time scales, can provide deep insights that may enable parsimonious descriptions of catchment rainfall-runoff responses [*Jakeman and Hornberger*, 1993; *McDonnell et al*., 2007], and achieve generalizations beyond individual catchments [*Falkenmark and Chapman*, 1989; *Sivapalan*, 2005]. The focus of the study is not necessarily to seek more detailed physically based understanding of individual processes, but to generate broader insights into the nature of streamflow variability at a holistic level through the development of an organized hydrological perspective [*Klemeš*, 1988] based on a synthesis of what is already known and built into standard conceptual models of catchment response.

In this paper, we use rainfall-runoff data from over 300 catchments across the U.S., and through a combination of data analysis and conceptual rainfall-runoff modeling we aim to: (i) bring out the diversity of the seasonal water balance of catchments located across the continent, (ii) develop a framework to characterize similarity and differences of seasonal water balance behavior amongst these catchments, (iii) use this framework to group the observed seasonal water balances into clusters exhibiting similar behavior, and (iv) test and elucidate the central role of the seasonal water balance in underpinning and linking several signatures of streamflow variability across a wide range of time scales and system states.

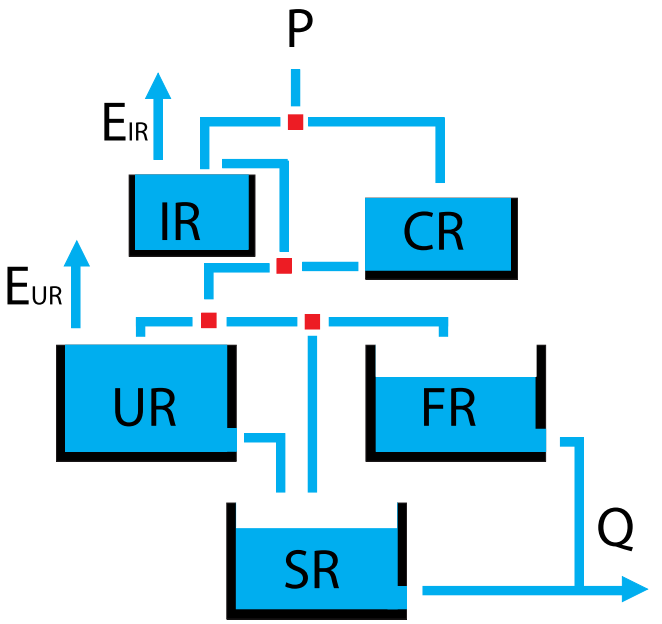

Figure 1. Structure of the extended $FLEX_I$ conceptual rainfall-runoff model used in this study (adapted from *Fenicia et al*. [2008]). The snow component of the model is adapted from *Eder et al*. [2003]. This model structure should be evaluated in conjunction with the model governing equations presented in Table 1. The model consists of five coupled stores representing snow (CR), vegetation interception (IR), unsaturated zone (UR), saturated groundwater (SR), and a store representing fast runoff (FR).

This study may be considered as an extension and also a synthesis of the previous work of *Kennard et al*. [2010], *Sawicz et al*. [2011], *Coopersmith et al*. [2012], and *Ye et al*. [2012]. *Sawicz et al*. [2011] used a Bayesian clustering scheme to group 280 U.S. catchments into nine homogeneous, hydrologically similar classes on the basis of a combination of six streamflow signatures. *Kennard et al*. [2010] also used Bayesian clustering scheme and hydrological signatures to obtain hydrologically coherent clusters in Australia. *Coopersmith et al*. [2012] developed a classification system to group a large and diverse population of catchments within the U.S. into homogeneous groups of similar seasonal streamflow variations. *Ye et al*. [2012] explored the dominant process controls of seasonal water balance in different parts of the U.S. through the use of a top-down modeling approach. In this paper, we extend the work of *Coopersmith et al*. [2012] and *Ye et al*. [2012] to arrive at a process-based similarity framework that includes the components of the seasonal water balance, including (model-predicted) seasonal variations of storage. The development of the similarity framework based on the seasonal water balance allows the clustering of similar catchments, supported by a deeper understanding of what makes these catchments similar. Consequently, the proposed delineation of hydrologically similar clusters extends from a purely empirical study [*Kennard et al*., 2010; *Sawicz et al*., 2011; *Coopersmith et al*., 2012], or a modeling study [*Ye et al*., 2012], to one based on holistic process understanding.

2. Methods

2.1. Constructing the Seasonal Water Balances

Through the use of a conceptual and parsimonious rainfall-runoff model, we reconstruct seasonal water balances of some 372 catchments located across the entire U.S. These catchments, which belong to the Model Parameter Estimation Experiment (MOPEX) data set [*Duan et al*., 2006; *Schaake et al*., 2006], span a wide diversity of climatic and physiographic characteristics and range in size from 67 to 10,329 km^2. Precipitation, temperature, potential evaporation, and streamflow are all available on a daily basis. Perennial snow cover is absent for most catchments and does not exceed 3% of the surface area for individual catchments [*Berghuijs et al*., 2014]. The MOPEX catchments are characterized by limited human influence [*Schaake et al*., 2006], which allows this study to focus on natural variability. The impact of anthropogenic factors, such as dams, is considered beyond the scope of this study.

Storage and evaporation components of the seasonal water balance are obtained through the implementation of the previously published $FLEX_I$ water balance model [*Fenicia et al*., 2008], now expanded with the snow module of *Eder et al*. [2003]. The model is of a lumped conceptual type and consists of stores representing the saturated and unsaturated soil zones, canopy interception and snow, and a surface store representing fast flow. Figure 1 presents the structure of the extended $FLEX_I$ model used here and Table 1

Table 1. Water Balance Equations for the Various Stores, Constitutive Relationships, and Description of Symbols[a]

Water Balance Equation	Constitutive Relationships	Description Symbols
CR : $\frac{dS_c}{dt} = R_c - P_c$	$R_c = P, \quad \text{if } T \le T_{crit}$ $P_c = \min(\max(T - T_{crit}, 0) \cdot f_{dd}, S_c/\Delta t)$	β = shape parameter (-) E_{IR} = interception evaporation [L/T] E_p = potential evaporation [L/T]
IR : $\frac{dS_i}{dt} = R_i - E_{IR}$	$E_{IR} = \min(E_p, S_i/\Delta t)$ $P_i = \min(S_i - I_r, 0)/\Delta t$ $R_i = P, \quad \text{if } T > T_{crit}$	E_{UR} = unsaturated zone evaporation [L/T] D = partitioning coefficient (-) f_{dd} = degree-day factor [L/T^2] I_r = storage capacity interception res. [L] K_f = time scale fast reservoir [1/T]
UR : $\frac{dS_u}{dt} = R_u - E_{IR}$	$C_r = \left(1 + \exp\left(\frac{-\frac{S_u}{S_{uc}} + \frac{1}{2}}{\beta}\right)\right)^{-1}$ $P_e = P_i + P_c$ $R_u = (1 - C_r) \cdot P_e$ $E_{UR} = (E_p - E_{IR}) \cdot (1, \frac{S_u}{S_{sf}} \frac{1}{L_p})$	K_f = time scale groundwater reservoir [1/T] L_p = evaporation threshold (-) P = precipitation [L/T] P_i = precipitation excess interception [L/T] P_m = max. percolation rate [L/T] R_i = recharge interception reservoir [L/T] R_c = recharge snow reservoir [L/T] R_f = recharge fast reservoir [L/T] R_s = recharge groundwater reservoir [L/T] R_u = recharge unsaturated reservoir [L/T]
SR : $\frac{dS_s}{dt} = R_s - Q_s$	$R_s = (P_e - R_u) \cdot D + P_m \cdot (S_u/S_{uc})$ $Q_s = \frac{S_s}{K_s}$	S_c = snow reservoir storage [L] S_I = interception storage [L] S_u = unsaturated reservoir storage [L] S_s = groundwater reservoir storage [L] S_f = fast reservoir storage [L] S_{uc}= storage capacity unsaturated reservoir [L]
FR : $\frac{dS_f}{dt} = R_f - Q_f$	$R_f = (P_e - R_u) \cdot (1 - D)$ $Q_f = \frac{S_f}{K_f}$	t = time (days) T = temperature (°C) T_{crit} = threshold temperature (°C) Q_f = discharge fast reservoir [L/T] Q_s = discharge groundwater reservoir [L/T]

[a]Please refer to Figure 1 for the model structure and the organization of the stores.

provides the coupled set of water balance equations included in the model, the associated constitutive relationships, and the definitions of the parameters.

The model is calibrated in each of the 372 catchments using the MOSCEM-UA algorithm [*Vrugt et al*., 2003] with 10,000 iterations. The model is calibrated for the period 1972–1977 using as objective functions the Nash-Sutcliffe efficiency [*Nash and Sutcliffe*, 1970] of the flow duration curve and the Nash-Sutcliffe efficiency of the logarithm of the flow. Because of the focus on seasonal water balance, the parameter sets with the best Nash-Sutcliffe fit to the observed regime curves (45 day moving average mean within-year variation of streamflow) for the 10 year period (1972–1982) are selected for further analysis. The 45 day time window is chosen to filter out most of the short-term and interannual variability of the observed hydrographs, but preserve most of the distinct seasonal behavior. For longer time periods, shorter time windows have been used to construct the regime curve [e.g., *Ye et al*., 2012]. Similar time windows provide noisy seasonal hydrographs when only 10 years of data are used. Most of the catchments produce a relatively smooth regime curve using the 45 day window that we have used. Of the 372 catchments, 51 catchments for which the Nash-Sutcliffe efficiency of the regime curves are smaller than 0.80 are removed from further consideration, in order to eliminate unrealistic and uncertain seasonal patterns. Figure 2 displays three examples of simulated and measured seasonal discharge regimes and associated Nash-Sutcliffe efficiencies (NS). The examples represent a good and clearly acceptable regime fit (NS = 0.95), a marginally acceptable regime fit (NS = 0.81), and a catchment with a poor fit, which was therefore rejected from any further consideration (NS = 0.54). In general, catchments in the agricultural mid west and in the relatively more arid zones have poorer model performances, and are the ones removed from contention. This is in line with the earlier modeling study of *Ye et al*. [2012]. At the multiannual scale, because carry-over of soil water and frozen water storage over several years can be assumed negligible, especially when the water year is used, calibrated model predictions of evaporation can be deemed accurate enough. On the other hand, although no storage or evaporation measurements are available to validate model predicted within-year variations of storage and evaporation, the spatial variations of seasonal water storage change between the months appear, to first order, to be in line with results of earlier studies [*Güntner et al*., 2007]. Clearly, the outcomes of this paper will rely critically on the performance and robustness of the model predictions,

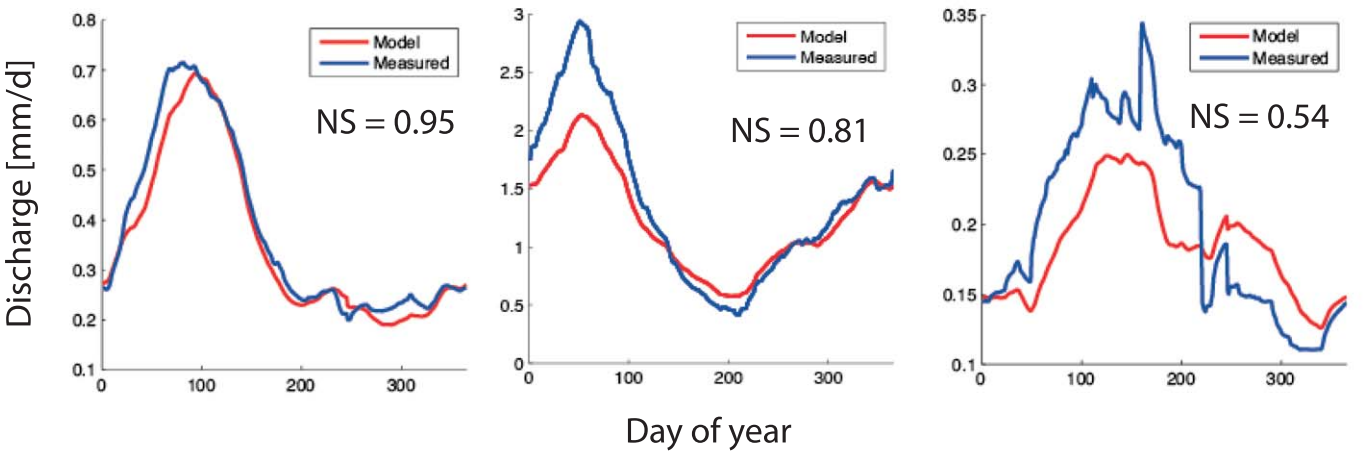

Figure 2. Three examples of simulated and measured seasonal discharge regimes and associated Nash-Sutcliffe efficiencies (NS). The catchments on the left and center have been accepted for further study (NS > 0.80). The discharge regime on the right is one of the 51 eliminated catchments because the model predictions had an unacceptable fit with the observed data (NS < 0.80).

and for this reason, they can be considered a plausible hypothesis that can continue to be refined in the future with further refinements to the model, improved estimation of parameters, and through conditioning with independent measurements, such as evaporation rates from flux towers, up-scaled to catchment scale [*Thompson et al*., 2011] and water storage variations from satellite gravimetry [*Lo et al*., 2010].

With the available data and the internal dynamics simulated by the model, we characterize the first-order seasonal water balance dynamics of the remaining 321 catchments: how much water is stored and what part is released, using the 10 year mean of the 45 day moving average of a simple mean seasonal water balance equation:

$$\frac{\Delta S_{ug}}{\Delta t}+\frac{\Delta S_s}{\Delta t}=P_n+P_s-Q-E_a \quad (1)$$

where P_n stands for rainfall (mm/d), P_s for snowmelt (mm/d), Q for streamflow (mm/d), E_a for evaporation (mm/d), S_{ug} for storage in the unsaturated zone and groundwater reservoir (mm), S_s for storage in the snow reservoir (mm), and t for time (day). In addition, we also define the water deficit D (mm/d), which is the difference between potential evaporation, E_p, and actual evaporation, E_a. Evaporation is a lumped flux combining all evaporative processes, including interception, soil evaporation, and transpiration. Combined storage in the unsaturated zone and in the groundwater reservoir is expressed as a relative storage of the catchment compared to the value on the first of January, which is fixed arbitrarily at 150 (mm) to allow intercomparison of catchment storage variations. Note that the model outcomes are solely used for the construction of seasonal water balances for the purpose of formation of clusters of similar catchments; the analysis of other signatures of streamflow variability will be based on measured streamflow data, not model predictions. The reconstruction of equation (1), through the use of multiyear model simulations, thus leads to the quantification of seven components of the mean seasonal water balance: P_n, Q, P_s, S_s, E_a, S_{ug}, D, as defined above. The mean within-year variations of these seven components will be the basis for defining similarity of seasonal water balances.

2.2. Constructing a Similarity Framework and Forming Coherent Clusters

Upon completion of the modeling and the quantification of the mean seasonal water balance for each of the catchments as per equation (1), the next tasks, using these model outputs, are the organization of these catchments into coherent groups on the basis of seasonal water balance similarity, followed by the identification of key physical controls of the seasonal water balance, to underpin the development of a quantitative similarity framework. These key tasks are undertaken in several steps.

First, all the individual seasonal water balances are presented on a national map. This map is used to visually explore the presence of coherent patterns in the seasonal water balances, and to compare these to results

of previous classification studies [e.g., *Coopersmith et al*., 2012; *Ye et al*., 2012; *Petersen et al*., 2012]. Guided by the previous studies and the characteristics of the clusters formed here, we look for climatic variables that may govern broad-scale patterns of the seasonal water balance dynamics. We then test the ability of several hydroclimatic indices (see later for details) governing both annual and seasonal water balances that have been previously proposed, i.e., by *Budyko* [1974] and by *Woods* [2009], to distinguish between classes of seasonal water balance behavior generated by the model. Finally, we experiment with variations of cluster boundaries through different combinations of the hydroclimatic indices and in this way form 10 hydrologically coherent clusters. This is done manually in an iterative manner until catchment clusters are formed that satisfy the key criteria of similarity within cluster (minimum within-cluster variance) and differences between (maximum between-cluster variance). The variance measure used here is the *RMSE-observations standard deviation ratio* [*Moriasi et al*., 2007].

2.3. Comparison of Streamflow Signatures at a Range of Time Scales

Using the clusters formed on the basis of the seasonal water balance, we subsequently investigate if and how the seasonal water balance is related to, underpins, or explains other streamflow signatures, looking for evidence of within-cluster similarity and between-cluster variability. These signatures reflect the functioning of catchments over a wide range of time scales (daily to decadal) and a wide range of states (low flows to floods). The signatures considered are the flow duration curve, the flood frequency and growth curves, the low flow frequency curve and decline curve, the base flow index, the rising limb density, the annual streamflow and interannual variability, and the long-term water balance in the context of the Budyko hypothesis [*Budyko*, 1974]. Note that these signatures are not explicitly accounted for in the previous clustering analysis but, together as a group, can be considered composite measures of the overall hydrologic functioning of the catchments [*Wagener et al*., 2007; *Sawicz et al*., 2011]. Note again that this comparative analysis of the various signatures is performed using actual streamflow observations, not model predictions.

3. Results

3.1. Regional Patterns of the Seasonal Water Balance

We begin with a presentation of the diversity of the mean seasonal water balances across the U.S., as predicted by the model. For illustration purposes, we present in Figure 3 the mean seasonal water balance regimes for just 17 selected catchments, distributed across the country. The remainder of the 321 catchments not displayed (purely due to space limitations) can be considered, with a few exceptions, as interpolations between the chosen 17 catchments.

The inset at the bottom left corner and the caption illustrates the kind of information that is used to describe the seasonal water balance regime. These include: the main input to the system (rainfall + snowmelt: red line), potential evaporation (dashed black line), snow storage (blue line), and soil water storage (bold black line). The magnitude of actual evaporation is represented by the size of the dark blue shading, and the magnitude of streamflow is represented by the size of the green shading. Note that all of the quantities presented above are ensemble means, over the 10 years of model simulation. Also note that the soil water storage is a relative magnitude, set to 150 (mm) on 1 January. We now use this template to interpret physically the mean seasonal water balance regimes for the 17 chosen catchments, in order to gain insights into the nature of variability across the continental U.S.

In the western part of the U.S., the catchments have a seasonal precipitation regime, with the peak of precipitation during winter (out of phase with potential evaporation). Consequently, these catchments have a large storage variation over the year. High winter precipitation is partially stored and released later and hence streamflow is seasonal. In the Pacific Northwest, the water deficit (the difference between potential and actual evaporation) is only present during the months with low precipitation and additionally, there is a significant influence of snow. In central and southern California, the aridity index is higher and the seasonality of streamflow is also stronger, and significant discharge is only observed during the winter period. In arid catchments, streams may fall dry during summer and have a large water deficit throughout most of the year.

Moving east, the mountainous catchments in the Rocky Mountains, Cascade Range, and Sierra Nevada have a very distinct snow influence. Again aridity and water deficit increase when moving south, and are experienced

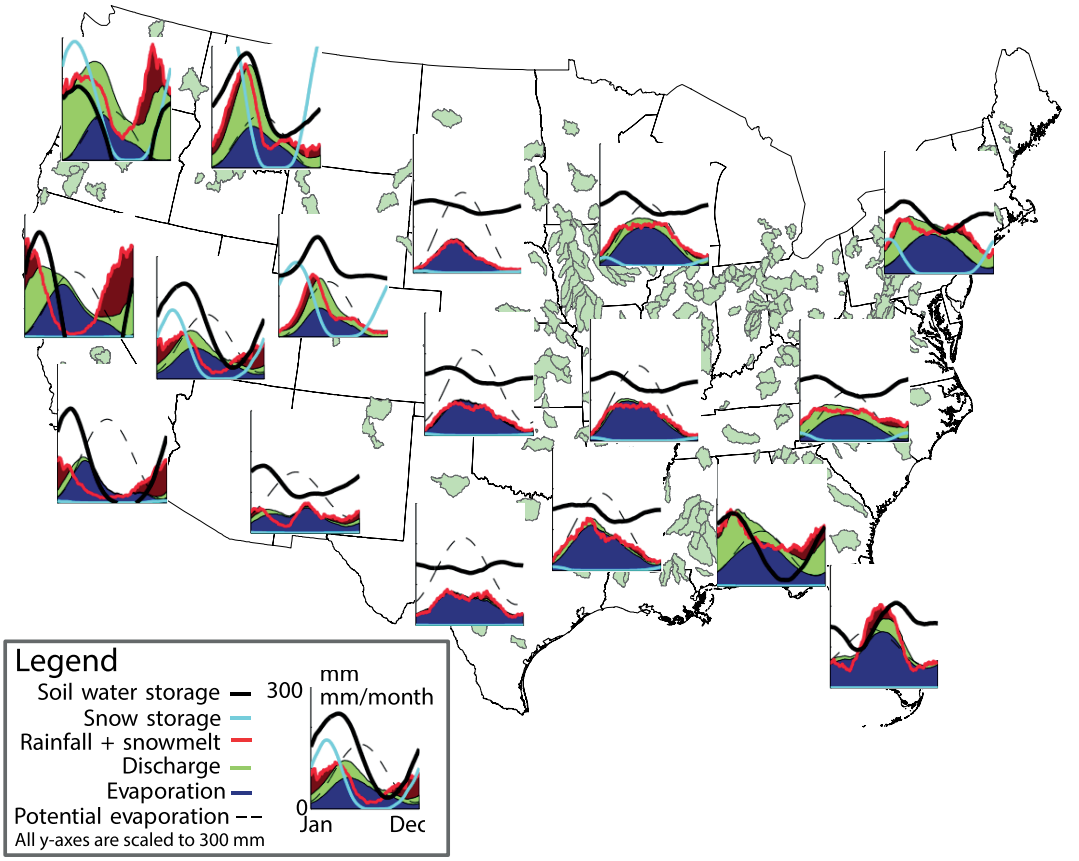

Figure 3. Diversity of the seasonal water balance across the U.S. represented by 17 catchments. Most of the seasonal regimes that are not displayed can be considered an interpolation of the displayed ones. Note that all *y* axes have the same scale.

throughout most of the year. Water availability and potential evaporation are more in phase, and snow accumulation on the surface and subsequent melt means less (and delayed) recharge to the soil below, leading to smaller soil water storage variation compared to the catchments in the western coastal states.

In the more arid catchments of the Great Plains, precipitation and evaporation are in phase, leading to very small storage variations and much smaller streamflows. In the interior lowlands east of the Great Plains, relatively small storage variation persists; however, catchments are less arid, leading to more streamflow. Overall, smaller storage fluctuations and reduced seasonal accumulation indicate that soil moisture storage is concentrated at the surface, and combined with random storm event occurrences, thus contributing to much temporal and spatial variability.

In the south-eastern part of the U.S., precipitation is seasonal. In Florida, a distinct increase in precipitation is observed during the summer months. A part of this water results in streamflow, but evaporation is high as well. Overall this increase in streamflow and evaporation does not match the precipitation and significant change in storage can be observed. In other south-eastern U.S. catchments, the presence of two small peaks in precipitation and lower precipitation during summer months leads to seasonality in discharge and significant storage variation. Catchments are relatively humid, and water deficit remains small during the summer months.

The eastern and north-eastern parts of the U.S. have relatively constant precipitation throughout the year, with a distinct increase of snow in the northern parts and parts of the Appalachian Mountains. These catchments do not have much water deficit, and the variation of water storage is relatively small. Discharge in Northern catchments is increasingly seasonal and out of phase with potential evaporation, but this is due to a combination of snowmelt and the phenology associated with deciduous forests [*Ye et al.*, 2012].

The above assessment of seasonal water balance has highlighted several facets of the enormous variability seen across the continental U.S.: total runoff volume, seasonal flow regime, seasonal soil water storage

regime, snow storage, and snowmelt. Preliminary assessment of the seasonal water balances of not just the 17 catchments, but all 321 catchments, indicate that, similar to *Coopersmith et al*. [2012] and *Ye et al*. [2012], spatial variations of climate seasonality and aridity underpin much of the wide diversity of the seasonal regimes exhibited by the MOPEX catchments. Aridity determines the partitioning of precipitation into evaporation and discharge. The timing of precipitation in relation to potential evaporation has a large impact on seasonal soil water storage and the discharge regime. Additionally, snowmelt and accumulation processes provide a distinct streamflow peak and delay in soil water recharge in the mountainous catchments in the west. Vegetation phenology (which, like snow, is partly temperature driven [*Thompson et al*., 2011]) contributes to the strong seasonality of streamflows in the north-east [*Ye et al*., 2012]. Overall, we identify the role of climate aridity, precipitation timing, snow, and phenology (also governed by temperature), as the primary controls of the seasonal water balances. Therefore, they are potential candidates to serve as quantitative indices to define similarity of seasonal water balances.

3.2. Similarity Framework for Seasonal Water Balance

On the basis of the assessment of the computed seasonal water balances, we propose three dimensionless indices that account for the key physical controls identified above: aridity, precipitation timing, and snowiness. To allow simple forms for these indices, we assume that the seasonal variability of precipitation, potential evaporation, and air temperature can be modeled as simple sine curves [*Milly*, 1994; *Potter et al*., 2005; *Woods*, 2009]. This assumption holds well for most regions in the U.S., although catchments in the south and south-west of the U.S. may be exceptions.

$$P(t) = \overline{P}\left[1+\delta_P \sin\left(2\pi\ \left(t-s_p\right)/\tau_P\right)\right] \tag{2}$$

$$E(t) = \overline{E}\left[1+\delta_E \sin\left(2\pi\ \left(t-s_E\right)/\tau_E\right)\right] \tag{3}$$

$$T(t) = \overline{T}+\Delta_T\left[\sin\left(2\pi\ \left(t-s_T\right)/\tau_T\right)\right] \tag{4}$$

where t is the time (days), s is a phase shift (days), τ is the duration of the seasonal cycle (days), δ is a dimensionless seasonal amplitude, Δ is the seasonal amplitude, and the subscripts T, P, and E stand for temperature, precipitation, and potential evaporation (mm/d). Duration τ of the seasonal cycle is 1 year $(\tau_T = \tau_P = \tau_E = 365\ \text{days})$. P(t) is the precipitation rate (mm/d) as a function of t, with the time-averaged mean value $\overline{P}$. E(t) is the potential evaporation rate (mm/d) as a function of t, with the time-averaged mean value $\overline{E}$. The temperature, T(t) has a time-averaged mean value $\overline{T}$ (°C), and seasonal amplitude Δ_T (°C). Using a least squares optimization, we obtain the coefficients of the equations for all individual catchments. From these equations, we adopt simple expressions for the seasonality and timing of precipitation, the aridity, and the fraction of precipitation falling as snow. With the variables presented in equations (2–4), we now define three dimensionless similarity indices, whose ability to characterize the similarity of seasonal water balances will be tested subsequently.

3.2.1. Seasonality and Timing of Precipitation

The similarity index governing the seasonality and timing of precipitation is defined as [*Woods*, 2009]:

$$\delta_P^* = \delta_P \cdot \text{sgn}\ (\Delta_T) \cdot \cos(2\ \pi(s_p - s_T)/\tau) \tag{5}$$

The dimensionless variable δ_P^* describes the seasonality of precipitation and whether or not the precipitation is in phase with the potential evaporation and temperature regimes ($s_T \approx s_E$). δ_P^* can range from -1 to 1, and represents the following scenarios:

1. $\delta_P^* = -1$, for strongly winter-dominant precipitation (out of phase with E_p or T).
2. $\delta_P^* = 0$, for uniform precipitation throughout the year.
3. $\delta_P^* = +1$, for strongly summer-dominant precipitation (in phase with E_p or T).

3.2.2. Fraction of Precipitation Falling as Snow

The fraction of precipitation falling as snow is the second similarity index. This fraction is both a function of temperature and δ_P^*, and is approximated by *Woods* [2009] as:

$$f_s = f_s\left(\overline{T^*},\ \delta_P^*\right) = \frac{1}{2} - \frac{\sin^{-1}\left(\overline{T^*}\right)}{\pi} - \frac{\delta_P^*}{\pi}\sqrt{1-\overline{T^*}} \tag{6a}$$

where $\overline{T^*}$ is a dimensionless measure of the mean temperature:

$$\overline{T^*} = \frac{\overline{T} - T_0}{|\Delta_T|} \tag{6b}$$

where T_0 is the critical temperature below which precipitation falls as snow, set at 1°C. The dimensionless similarity index f_s can range from 0 (all precipitation falls as rain) to 1 (all precipitation falls as snow).

3.2.3. Aridity Index

The dimensionless aridity index is approximated by *Budyko* [1974] as:

$$\varphi = \frac{\overline{E}}{\overline{P}} \tag{7}$$

where $\overline{E}$ is the mean potential evaporation rate (mm/d) and $\overline{P}$ is the mean precipitation rate (mm/d), where the mean is estimated over many years. φ can range from 0 to (in theory) infinity.

3.2.4. Overview of the Similarity Framework

The three proposed hydroclimatic indices (δ_P^*, f_s, φ) span a three-dimensional space, which is presumed to accommodate most of the spatial variability in the observed seasonal water balances. Figure 4 displays the framework, including a qualitative description of how some of the key components of the seasonal water balance change due to gradients in the proposed indices. To first order, the aridity index determines the long-term partitioning of incoming precipitation into streamflow and evaporation. The timing and seasonality of precipitation, in relation to those of potential evaporation, determines not only the within-year variation of streamflow, but also rates of accumulation and subsequent release of soil moisture and groundwater storage. An increased fraction of precipitation falling as snow contributes to the accumulation of snow during the cold winter period, a delay in contributions to soil moisture and recharge to groundwater, and the subsequent melting during spring, which contributes to higher delayed streamflows during this time of the year. In the east and north-east, a high value of f_s also coincides with the presence of deciduous vegetation, which responds to the wide variations of temperature through large changes of phenology: dropping of leaves and minimal evaporation during winter and greening up and vigorous evaporation during spring and summer.

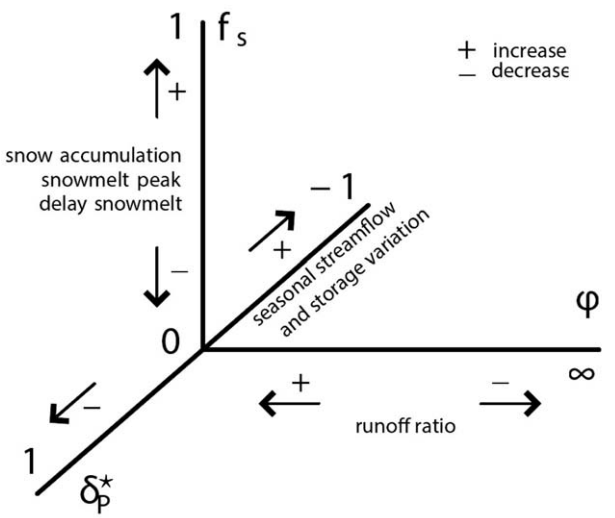

Figure 4. The proposed framework consisting of three hydroclimatic indices. δ_P^* expresses the seasonality and timing of precipitation, f_s the fraction of precipitation falling as snow, and φ the aridity index. The figure includes descriptions of how key processes of the seasonal water balance change as a function of the indices.

The spatial distributions of δ_P^*, f_s, φ, are displayed in Figures 5a–5c. Each of the three indices exhibits distinct regional patterns, generally independent of each other. Most of the catchments in the east and in the north-west tend to be generally humid, with low values of the aridity index, φ, whereas catchments in the midsection of the continent as well as in the south-west are generally semi-arid to arid with higher values of φ. In the case of precipitation timing, catchments in the east tend to have low-precipitation seasonality with values of δ_P^* in the range [−0.4, 0.4], whereas the catchments in the midsection of the continent (Great Plains, Central Plains)

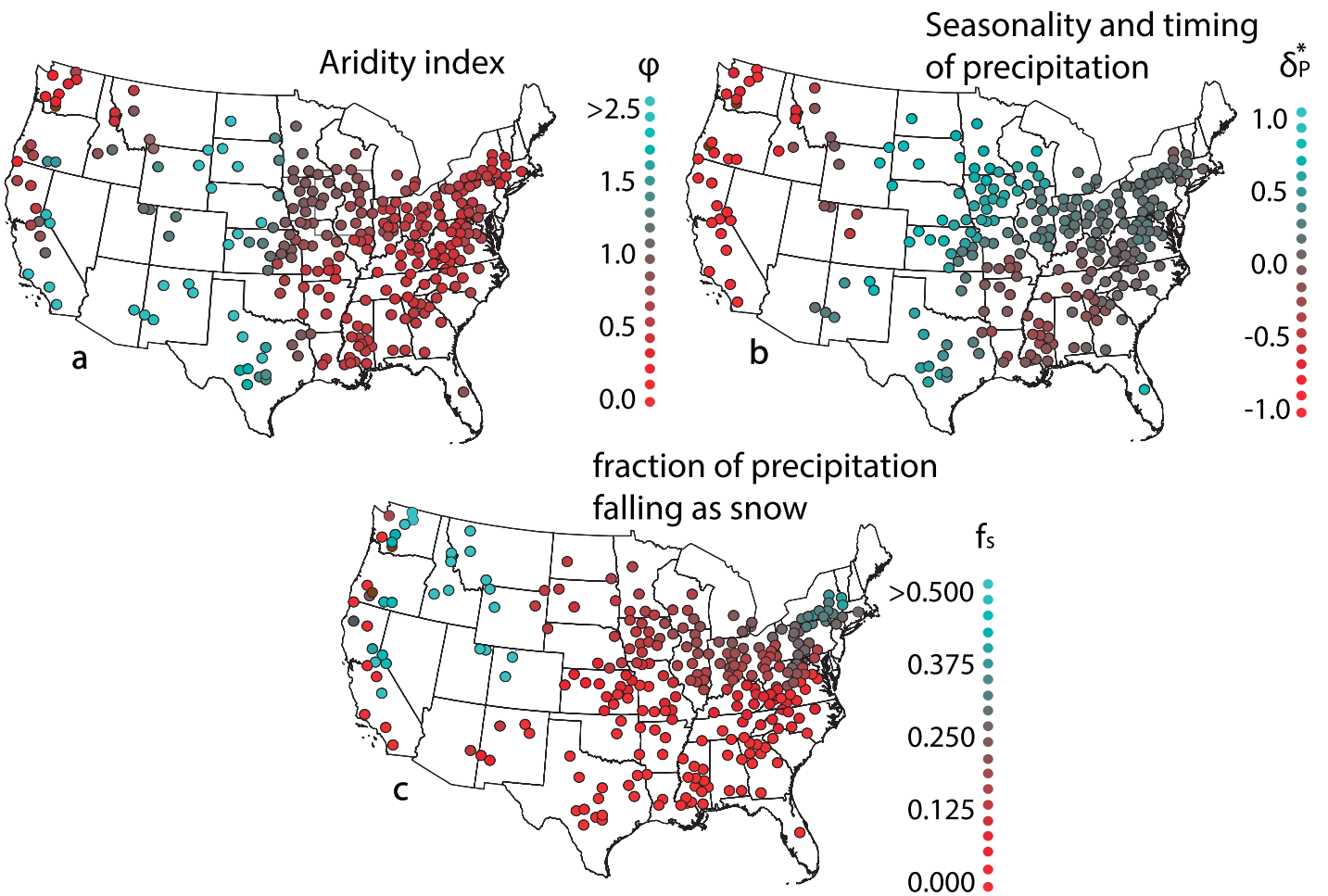

Figure 5. The values of the hydroclimatic indices δ_p^* (measure of precipitation timing with respect to potential evaporation), f_s (snowiness, fraction of total annual precipitation that falls as snow), and φ (aridity index, ratio of annual potential evaporation to annual precipitation) for the 321 study catchment catchments.

exhibit in-phase seasonality with δ_p^* values approaching 1.0, and catchments in the west exhibit strong out-of-phase seasonality with δ_p^* values approaching -1.0. Finally, the patterns of f_s show that catchments in the north-east and mountainous catchments along the Rockies, Cascade Range and Sierra Nevada have snowfalls exceeding 50%, whereas most of the rest of the catchments have lower to negligible snowfall as a fraction of total precipitation. The ability of these three independent hydroclimate indices to characterize the similarity and differences of the computed seasonal water balances of the 321 study catchments is explored next.

3.3. Grouping of Catchments Into Coherent Clusters

The objective here is to group the 321 study catchments into a small number of hydrologically coherent clusters on the basis of the seven components of the mean seasonal water balance, namely, P_n, Q, P_s, S_s, E_a, S_u, and D. In this study, the grouping is done manually through a trial and error procedure based initially on visual observations, which is then refined by an iterative procedure. This is achieved by progressively adjusting the boundaries between the resulting clusters in terms of the three climatic similarity indices defined before, through the application of objective criteria (minimum within-cluster variance and maximum between-cluster variance). Here only the results relating to the final cluster configurations are presented.

Figure 6 presents the seasonal variations of these same seven components for catchments belonging to each of the resulting final 10 catchment clusters. Regimes of individual catchments are displayed using thin lines, while the average value within the cluster is presented using a thicker black line. These displays can

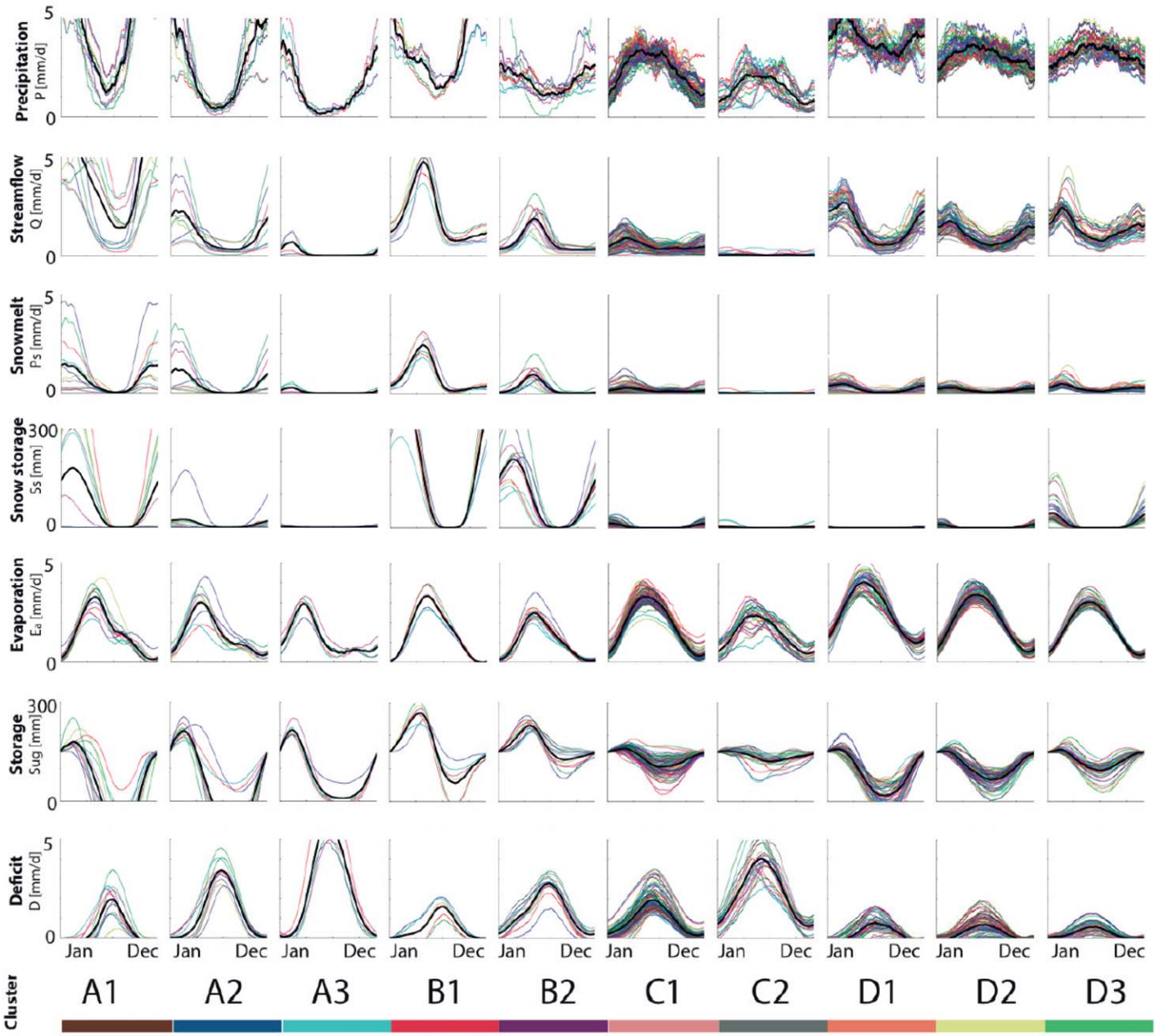

Figure 6. Overview of the fluxes and storage regimes of the 10-catchment clusters. Regimes included are (first row) the precipitation, (second row) streamflow, (third row) snowmelt, (fourth row) snow storage, (fifth row) evaporation, (sixth row) storage, and (seventh row) deficit. The thin colored-lines display values of the individual catchments. The thicker black lines display the within-cluster average values. (Note that some values are not shown because they plot above the top of the vertical scale.)

already be used to visually assess the degree to which these seven components of seasonal water balance show similarity and differences, both within and between the clusters. There is much that can be learned from Figure 6 about the richness of seasonal water balances across the U.S.: not only the differences between the clusters, but in some cases even the variability within some of the clusters themselves. One way to frame this discussion is to chart how the variability in the precipitation propagates through the catchments and ends up in the observed streamflow variability. First row of Figure 6 shows that there is considerable variation in the seasonal precipitation regime between the clusters: from a large snowmelt component (B1, B2), out-of-phase seasonality of P with E_p (A1, A2, and A3), in-phase seasonality (C1, C2), mild to no seasonality (D2, D3) to mild out-of-phase seasonality (D1). These propagate to wide variations in the snow and soil water storage and streamflow. In B1 and B2, snow storage is more dominant than soil

water storage, and spring snowmelt dominates streamflow. A1, A2, and A3 experience large seasonal soil water storage variations, and winter flows dominate streamflow. Due to in-phase seasonality, the range of seasonal soil water storage is very low in C1 and C2, and streamflow is mildly seasonal with dominant winter flows. There is also considerable within-cluster variability in C1 and C2 compared to the more western clusters, perhaps pointing to the dominance of local, event-scale responses, and potentially also caused by differences in soils, or land cover and land management in these major agricultural regions. Clusters D2 and D3 show that the slightly (or no) in-phase seasonality of precipitation is transformed to strong out-of-phase seasonality of streamflow. This is a combined result of snowiness and a strong impact of vegetation phenology. Finally, D1 represents a more straightforward transformation from out-of-phase precipitation to out-of-phase seasonality of streamflow. In spite of these large variations across the continent, the seasonal regimes of actual evaporation show considerable similarity in both shape and magnitude amongst all clusters, less so for the dry catchments (e.g., A2, A3). This is interesting, considering that the clusters cover a broad range of climates and landscape properties, including vegetation. Granted, this is a model predicted result, yet these rates when aggregated to the annual time scale are still correct, because the model is calibrated against observed streamflows. This comes across as an emergent pattern, and raises the question as to whether any of this can be explained by adaptation of the catchment (and vegetation) with climate. This calls for further detailed study, with the use of not only measured evaporation rates in different parts of the continent but also estimates of vegetation cover and net primary productivity, guided by large-scale theories governing long-term water balances and vegetation behavior, including the Budyko and Horton Hypotheses [*Budyko*, 1974; *Troch et al*., 2009].

Even though visual inspection of the results presented in Figure 6 indicate remarkable similarity within, and significant differences between, the 10 catchment clusters, can this be objectively confirmed? In order to assess this quantitatively, we estimated the *RMSE-observations standard deviation ratio* (abbreviated as RSR) [*Moriasi et al*., 2007] for the seven different components of the seasonal water balance ($P_n, Q, P_s, S_s, E_a, S_u, D$) of individual catchments, compared to the mean regimes of that component of a certain cluster, given by:

$$RSR_M^K = \frac{1}{n}\sum_{n=1}^{N}\frac{1}{7}\sum_{m=1}^{7}\frac{\sqrt{\sum_{i=1}^{365}(X_i^{m,n}-Y_i^{\overline{m}})^2}}{\sqrt{\sum_{i=1}^{365}(X_i^{m,n}-\overline{Y^m})^2}} \quad (8)$$

where n is the catchment under consideration, N is the number of catchments present in that cluster, M is the cluster under consideration (M = 1:10; A1, A2, A3, B1, B2, C1, C2, D1, D2, D3), K is the cluster to which a catchment from cluster M is compared (K = 1:10; A1, A2, A3, B1, B2, C1, C2, D1, D2, D3), m is the regime of consideration (m = 1 : 7; $P_n, Q, P_s, S_s, E_a, S_u, D$), i is the day of year (i = 1:365), $X_i^{m,n}$ is the value of the regime m from catchment n on day i from cluster M, $Y_i^{\overline{m}}$ is the mean of the N regime curves from cluster K and $\overline{Y^m}$ is the mean value of $Y_i^{\overline{m}}$. The resulting RSR_M^K is a measure of how large is the average variance between cluster M and the mean of cluster K. Values of the RSR_M^K for each of the 100 cluster pairs are presented in Table 2. The results show that indeed the estimates of RSR_M^K are the lowest along the diagonal of Table 2, which represent the variance within, whereas the off-diagonal terms that represent variance between are all larger. This confirms that the 10 chosen clusters are indeed hydrologically coherent and possibly having distinct characteristics, both visually and objectively. Of course there is still considerable variability within some of the clusters. Likewise, both visual inspection and the magnitudes of the off-diagonal terms in the RSR_M^K table show that differences between the clusters D1, D2, and D3 are relatively small, even though they are still larger than the diagonal values. There is also a discrepancy in that D2 and D3 appear to be similar in terms of these metrics: both are affected by phenology and snow, yet to different degrees.

In order to place the 10 catchment clusters within the similarity framework proposed above, based on the three similarity indices, δ_P^*, f_s, φ, as part of the clustering procedure, we determined the combinations of the ranges of values of δ_P^*, f_s, φ, that apply to each of the 10 distinct clusters. These are presented in Table 3, which also contains a brief description of the nature of the within-cluster seasonal water balance, including, in each case, our initial interpretation of the dominant feature that controls the seasonal patterns of hydrological response. Figure 7 shows the geographic spread and organization of the 10 catchment

Table 2. The RSR_M^K Values of the Catchment Clusters[a]

	A1	A2	A3	B1	B2	C1	C2	D1	D2	D3
A1	0.58	0.88	0.98	0.88	0.98	0.92	0.89	0.82	0.85	0.87
A2	0.82	0.65	0.92	0.81	0.94	0.93	0.91	0.85	0.87	0.91
A3	1.00	0.80	0.53	1.11	1.08	0.95	1.01	0.91	0.96	0.99
B1	0.91	0.94	1.02	0.39	0.72	0.92	0.88	0.89	0.90	0.90
B2	1.06	1.22	1.23	0.98	0.52	0.97	0.95	1.05	1.02	1.01
C1	1.14	1.31	1.68	1.63	1.17	0.75	0.95	1.07	0.99	0.97
C2	1.12	1.53	1.34	1.41	1.28	0.82	0.58	1.00	0.82	0.8
D1	1.22	1.07	1.01	1.33	1.17	0.96	0.88	0.54	0.69	0.75
D2	1.27	1.49	1.17	1.56	1.37	0.91	0.8	0.87	0.55	0.64
D3	1.33	1.52	1.17	1.78	1.42	0.87	0.82	0.96	0.65	0.53

[a]The first row contains the M clusters and the first column the K clusters. The results show that the estimates of RSR_M^K are the lowest along the diagonal of Table 2, which represent the variance within, whereas the off-diagonal terms that represent variance between are all larger.

clusters obtained in this way; they exhibit remarkable spatial coherence. Figure 7 also displays the ranges of the climatic similarity indices δ_P^*, f_s, φ, that delineate the clusters, which emphasizes the role of seasonal climate in underpinning the seasonal water balances and associated dominant processes, regardless of landscape properties.

Having established the coherence and geographic location of the 10 chosen clusters and their connection to the three climatic indices, we next explore whether the locations and geographic spread of the clusters are mirrored in any on-ground features. Figure 8 presents the well-established ecosystem regions, soil orders, and locations of broad-scale plant formations across the continental U.S., in each case overlain by the locations of the 321 catchments and the clusters to which they belong. The results show a remarkable match between the locations and regional spread of the catchment clusters and the physiographic regions and plant formations, which not only supports the notion that the formation of local soils and vegetation is climate dependent, but also that vegetation and soils both contribute to and are a reflection of the seasonal water balance regime. The dominant features attributed to each of the catchment clusters in Table 3, can thus be deemed as mechanisms through which vegetation and soils adapt to and modify the seasonal water balance in each case. It must also be noted that although MOPEX catchments are characterized by limited anthropogenic influences [*Schaake et al*., 2006], some of the catchments in classes C1 and C2 are partly covered by cropland and pasture.

3.4. Connection to Similarity of Streamflow Signatures

Now that we have formed coherent clusters of catchments based on the seasonal water balance, each with distinct dominant seasonal processes, we explore their possible imprint on signatures of streamflow variability at a range of time scales. The variability of each signature within and between the clusters is examined, including any connections between these various signatures and aspects of the seasonal water balance. Note again that these signatures are derived directly from streamflow observations and not model predictions. The results are presented in descending order of time scales (annual, seasonal, daily), and extreme states (floods and low flows). While one would expect to see the manifestation of only the net effects of seasonality at the annual scale, the nature of climate seasonality can be expected to be explicitly manifested in streamflow variability at the seasonal scale. On the other hand, not all local (spatial) or short time scale variability can be accommodated in mean seasonal water balance behavior, and therefore is likely to show up as additional variability or "noise."

3.4.1. Mean Annual Water Balance and Interannual Variability of Streamflow

Figure 9 presents (top) the mean annual runoff ratio, and (middle) the coefficient of variation (CV) of the annual runoff ratio, i.e., the standard deviation of the annual runoff ratio divided by the mean runoff ratio. Note that clusters are organized here from the left to the right through a combination of aridity and seasonality (wet-dry-wet, out-of-phase, in-phase, no seasonality), in order to capture the gradient in dominant processes (and therefore, the order is different from what appears in Figures 6 and 11). Due to this organization, the results in Figure 9 (top) indicate that the mean annual runoff ratio initially decreases from the left to the right, hitting a minimum for cluster C2, and then increasing again toward the right. Correspondingly, the mean CV of annual runoff ratio shows an opposite trend: initially increasing from the left to the right

Table 3. Characteristics of the 10-Catchment Clusters[a]

Cluster	A1	A2	A3	B1	B2
Vegetation	Coniferous	Coniferous/Shrubs	Shrubs	Coniferous	Coniferous
Ecoregion	Marine mountains/Mediterranean regime mountains	Mediterranean regime mountains	Mediterranean regime mountains	Temperate steppe regime mountains	Temperate steppe regime mountains
Soil order	Andisols, inceptisols	Alfisols, inceptisols	Mollisols	Andisols	Entisols, inceptisols
Dominant process	Seasonal soil water storage	Seasonal soil water storage	Seasonal soil water storage	Snow storage	Snow storage
n	9	5	7	6	13
δ_P^*	−1/−0.4	−1/−0.4	−1/−0.4	−1/0	−1/0
Observed	−0.99/−0.83/−0.59	−0.99/−0.94/−0.90	−0.99/−0.83/−0.68	−0.90/−0.63/−0.35	−0.99/−0.39/−0.02
f_s	0/0.45	0/0.45	0/0.45	0.45/1	0.45/1
Observed	0/0.25/0.44	0/0.12/0.38	0/0.15/0.41	0.52/0.56/0.59	0.46/0.54/0.69
φ	0.35/0.75	0.75/1.75	1.75/5	0.4/0.75	0.75/1.75
Observed	0.36/0.41/0.64	0.76/1.00/1.54	1.83/2.60/4.10	0.42/0.57/0.73	0.83/1.32/1.74
Description	Humid catchments where precipitation and evaporation are out of phase. Consequently, large soil water and streamflow variations occur and streamflow is perennial.	Semiarid catchments where precipitation and evaporation are out of phase. Consequently, large soil water and streamflow variations occur and streamflow can be perennial or intermittent.	Arid catchments where precipitation and temperature are out of phase. Consequently, soil water and streamflow variations occur and streamflow can be intermittent.	Mountainous humid catchments where snow storage causes a delay in the streamflow and soil water recharge peak. Catchments have perennial streamflow	Mountainous semiarid catchments where snow storage causes a delay in the streamflow and soil water recharge peak. Catchments have perennial streamflow
Cluster	C1	C2	D1	D2	D3
Vegetation	Some short grass prairie, but mainly long grass prairie	Short grass prairie	Mixed deciduous coniferous	Deciduous	Deciduous
Ecoregion	Prairie	Steppe	Subtropical	Hot continental (Mountains)	Warm continental (Mountains)
Soil order	Mollisols	Mollisols/Aridisols	Utisols	Alfisols	Alfisols/Inceptisols/Spodosoils
Dominant process	Event-scale response	Event-scale response	Soil water storage	Phenology	Phenology and snow storage
n	48	30	69	83	51
δ_P^*	0/1	0/1	−0.4/0.3	−0.1/0.3	−0.1/0.4
Observed	0.02/0.47/0.73	0.15/0.56/0.90	−0.26/−0.03/0.21	−0.07/0.17/0.28	−0.01/0.25/0.39
f_s	0/0.25	0/0.25	0/0	>0/0.20	0.2/0.45
Observed	0/0/14/0.21	0/0.07/0.17	0/0/0	0.02/0.12/0.20	0.20/0.25/0.39
φ	0.9/1.5	1.5/5.3	0.5/0.9	0.5/0.9	0.4/0.9
Observed	0.91/1.13/1.43	1.56/2.38/5.29	0.53/0.68/0.71	0.51/0.74/0.90	0.46/0.64/0.89
Description	Semiarid catchments where precipitation and evaporation are in phase. Streamflow and storage variations of both soil water and snow are small. Streams may fall dry but can be perennial	Arid catchments where precipitation and evaporation are in phase. Seasonal streamflow and storage variations of both soil water and snow are very small. Streams are intermittent	Humid catchments where precipitation and evaporation are slightly out of phase. Catchment have soil water storage variations and a slightly seasonal streamflow regime with low flows during summer	Humid catchments where precipitation and evaporation are slightly in phase. Catchments have small soil water storage variations and a fairly constant seasonal streamflow regime.	Humid catchments where precipitation and evaporation are slightly in phase. Catchments have soil water and snow storage variations with a soil water and streamflow increase in spring.

[a]The table contains the cluster name, the dominant vegetation type [*Stephenson*, 1990], ecoregion [*Bailey*, 2009], soil order [*U.S. Soil Taxonomy*, 2014], number of catchment of within-cluster catchments (n), the clusters-boundary conditions (δ_P^*, f_s, φ), and associated observed minimum, average, and maximum values within the clusters. Additionally, a short description of the catchment's seasonal climate and hydrology is included.

AGU Water Resources Research

10.1002/2014WR015692

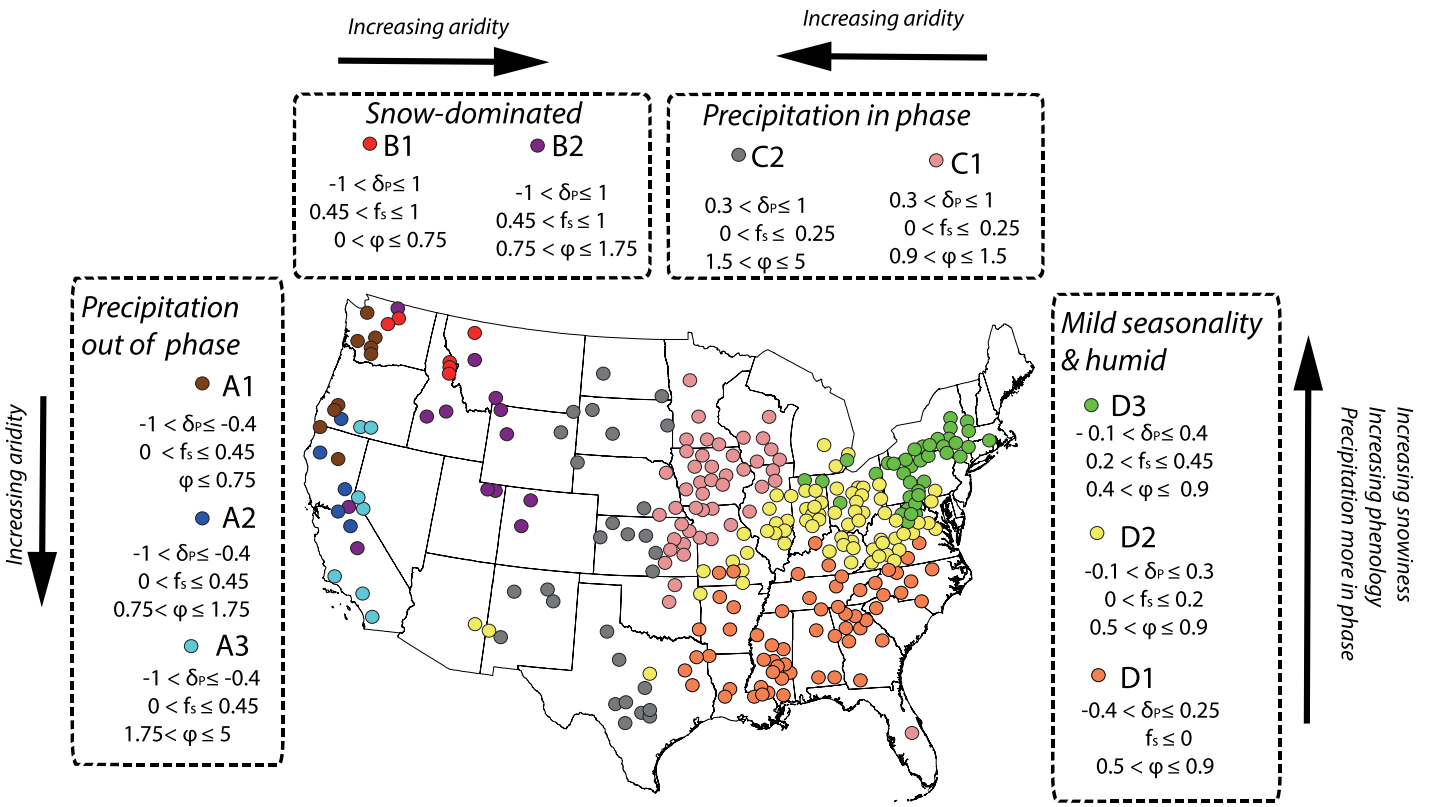

Figure 7. The organization of the 321 MOPEX study catchments into 10 hydrologically similar catchment clusters. The dotted boxes contain the description of the catchment classes, index ranges (δ_P^*, $\mathbf{f_s}$, φ), and the hydroclimatic character. Arrows describe changes in the hydroclimatic controls.

and then decreasing again. These changing but consistent patterns between the clusters are mostly due to change in aridity: clusters A3 and C2 (both arid regions) exhibit the smallest mean annual runoff ratio and largest mean CV. In addition, the within-cluster variability also exhibits the same or similar pattern as the mean CV: it first increases from left to right, and then decreases. Clusters A3 and C2 both exhibit the largest within-cluster variability. These trends are a consequence of a combination of aridity and intraannual variability of precipitation timing, and the presence or absence of snow.

To separate the effects of aridity, precipitation timing, and snow, we present in Figure 9 (bottom) the mean annual water balances of the study catchments on the Budyko curve [*Budyko*, 1974] as a function of the aridity index, but organized by cluster. The results in Figure 9 (bottom) shows that the mean annual water balances of individual catchments do indeed fall around the Budyko curve, but with large deviations. There is considerable organization to this scatter, however, in terms of the positions of the various clusters. Similar to previous studies [*Hickel and Zhang*, 2006], we find that timing of precipitation does have an impact on mean annual water balance. While clusters C1, D1, and D2 fall right on the Budyko curve or close to it, clusters A1, A2, A3, B1, B2, and D3 fall away (below) from the Budyko curve, producing more runoff (to different degrees) than predicted by Budyko. Differences between D1, D2, and D3 are due to differences in phenology and snowiness. Deviations from the Budyko curve are greatest for the mountainous clusters B1 and B2. In other words, the presence of snow increases annual runoff, i.e., $(B1,\ B2\colon\ f_s > 0.45;\ D3\colon f_s > 0.2)$, which is in line with the earlier findings of *Berghuijs et al.* [2014]. The semiarid and arid clusters with seasonal precipitation and precipitation in phase with potential evaporation, i.e., $\left(C1,\ C2\colon AI > 0.9,\ \delta_P^* > 0\right)$, have significantly less runoff (i.e., more evaporation) compared to Budyko's prediction. This is in contrast to catchments with precipitation out of phase with potential evaporation, i.e., $\left(A1,\ A2,\ A3\colon\ \delta_P^* < -0.3\right)$, which generate slightly more runoff than predicted.

3.4.2. Base Flow Index and the Rising Limb Density

The rising limb density is defined as the ratio of the number of rising limbs to the total length of time the hydrograph is rising [*Shamir et al.*, 2005]. A high rising limb density value indicates flashy hydrographs. The

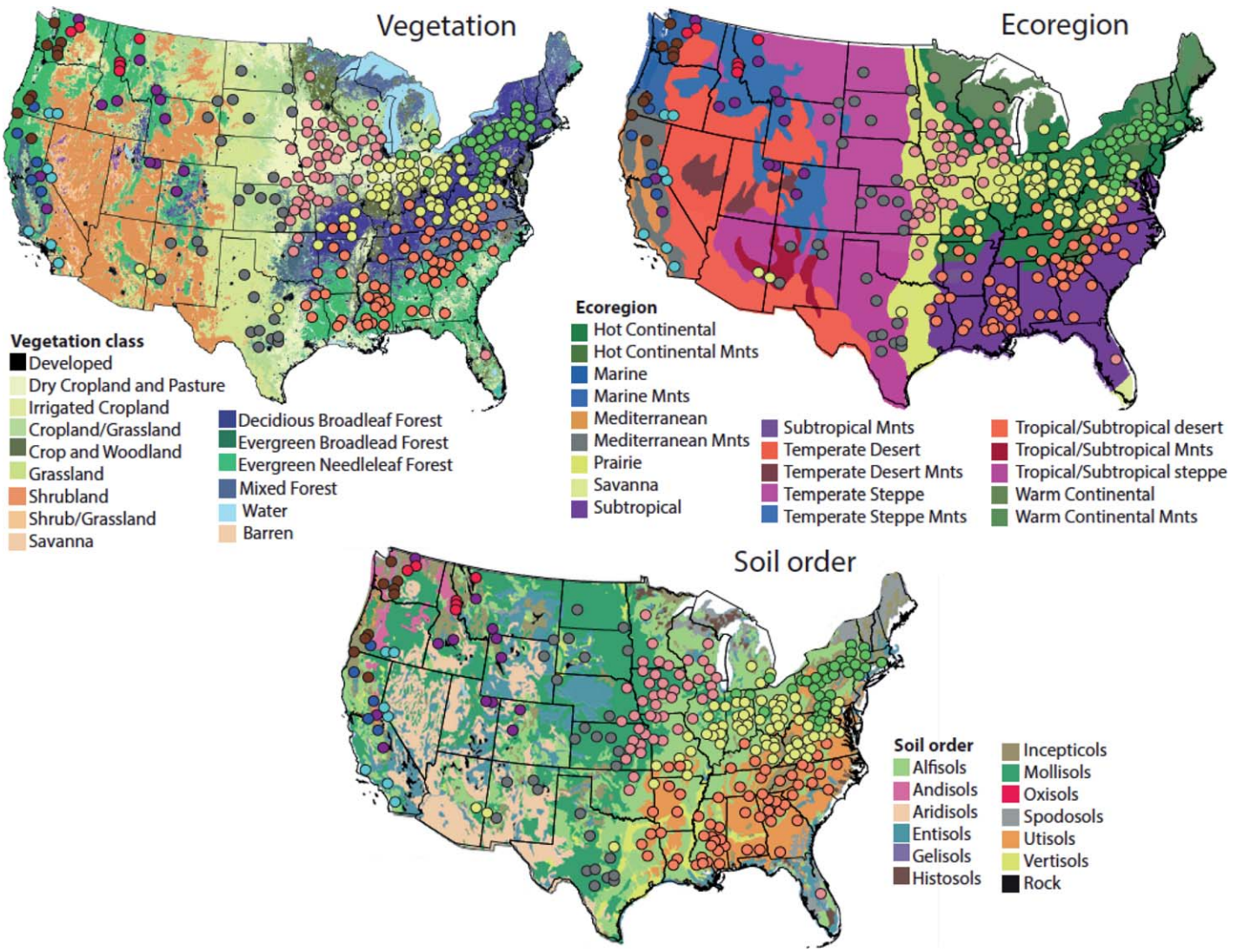

Figure 8. The organization of the ecosystem regions, main plant formations, and soil orders across the U.S. overlain by the locations of catchments belonging to the 10 catchment clusters.

base flow index is the ratio of long-term base flow to total streamflow; in this case, the base flow is estimated from the observed streamflow hydrograph through the application of a low-pass filter [*Arnold et al*., 1995; *Vogel and Kroll*, 1992; *Kroll et al*., 2004]. In a sense these are complementary features, the rising limb density is an indicator of frequency of fast flows, and base flow index is a measure of the importance of slow flows. We use the one-parameter single-pass digital filter method and associated parameters based on previous studies [e.g., *Arnold et al*., 1995; *Eckhardt*, 2008; *Sawicz et al*., 2011] to estimate the base flow index. Figure 10 displays the rising limb density and base flow index for the 10 catchment clusters. The base flow index is highest in the catchments dominated by snowmelt only $(B1,\ B2\colon\ f_s > 0.45)$ and lowest in the flat, semiarid, and arid catchments where small storage variability occurs $\left(C1,\ C2\colon AI > 0.9,\ \delta_p^* > 0\right)$. Catchments with a high rising limb density also have a low base flow index, and vice versa. Landscape controls play a vital role in determining both the base flow index and rising limb density, with strong differences between the mountainous catchments in the west and the flatter catchments in the mid west and the east. The results on the base flow index here agree with the regional patterns presented in *Beck et al*. [2013].

3.4.3. Seasonal Flow Regime and Pardé Coefficient

Figure 11 presents several signatures of variability at a range of time scales, from seasonal to daily, including floods and low flows. Figure 11 (first row) displays the Pardé coefficients [*Pardé*, 1933] that express the

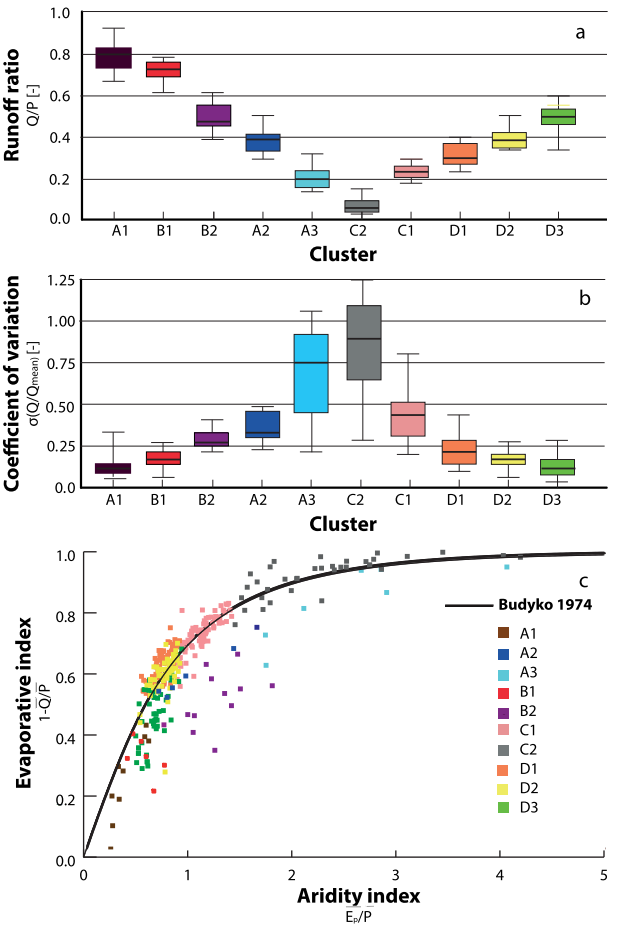

Figure 9. (top) The annual runoff ratio, (middle) the coefficient of variation of the annual runoff ratio, (bottom) and the long-term water balances presented in context of the Budyko Hypothesis [*Budyko*, 1974] for the 10-catchment clusters.

nondimensionalized seasonal flow regime of the catchments. The catchments with most precipitation falling as snow ($B1$, B2: $f_s > 0.45$) have a distinct streamflow peak during spring. Arid and semiarid catchments, with precipitation and potential evaporation in phase, $(C1, C2: AI > 0.9, \delta_P^* > 0.0)$, have the greatest within-class variability of flow regimes. Maximum flow in many catchments occurs in different winter or spring months, but for the arid catchments of C2, this peak in some cases observed during summer as well. This is not surprising, given the high variability of the precipitation regime shown in Figure 6, for these clusters. For catchments where precipitation and evaporation are out of phase $(A1, A2, A3: \delta_P^* < -0.3)$ the streamflow is highly seasonal (mostly winter flows), with the seasonal variability becoming increasingly skewed with increasing aridity. The seasonal flow regimes of clusters D1, D2, D3 are relatively similar, but for different reasons. The seasonal patterns of D1 simply reflect the precipitation pattern (which is mildly seasonal and out of phase with potential evaporation), whereas the seasonal flow regimes of D2 and D3 are more a reflection of vegetation phenology and snow storage. Overall, one can see that there is a clear imprint of the seasonal water balance in the Pardé coefficients, which is to be expected.

3.4.4. The Flow Duration Curve

The flow duration curve (FDC) is a representation of the frequency distribution of streamflow defined for a specific time step, usually daily [*Vogel and Fennessey*, 1995]. Figure 11 (second row) presents the FDCs for individual catchments (thin lines) and the average value within the cluster (thicker black line) for the daily discharge values. Note that the FDC is a frequency domain representation of daily flow variability, and the timing of flow is lost during its presentation. Nevertheless, in most of the clusters, a clear imprint of the seasonal water balance is still present in the FDCs. The catchments with most precipitation falling as snow ($B1$, B2: $f_s > 0.45$) show compact FDCs with a distinct inflection point. This inflection represents the differences between the period in spring when the winter snowpack is melting and the rest of the year. Arid and semiarid catchments, with precipitation and potential evaporation in phase, $(C1, C2: AI > 0.9, \delta_P^* > 0)$, may become dry during part of the year because there are marginal soil water storage variations that can buffer dry periods. These two clusters also show significant variability within the clusters, reflecting the seasonal variability of precipitation regimes (Figure 6) and flow regimes (Figure 11). In semiarid and arid catchments where precipitation and evaporation are out of phase, $(A2, A3: AI > 0.75, \delta_P^* < -0.3)$, the river dries out during the summer period because the soil water storage recharged during winter and the winter snowpack cannot provide sufficient base flow for the entire arid summer period. Overall, several clusters show remarkable similarities of the FDCs, e.g., D1, D2, D3. Also, sometimes it is hard to distinguish the cluster to which a catchment may belong on the basis of the FDC alone. This equifinality is a consequence of the frequency domain representation of the FDCs: two different types of within-year variability can give rise

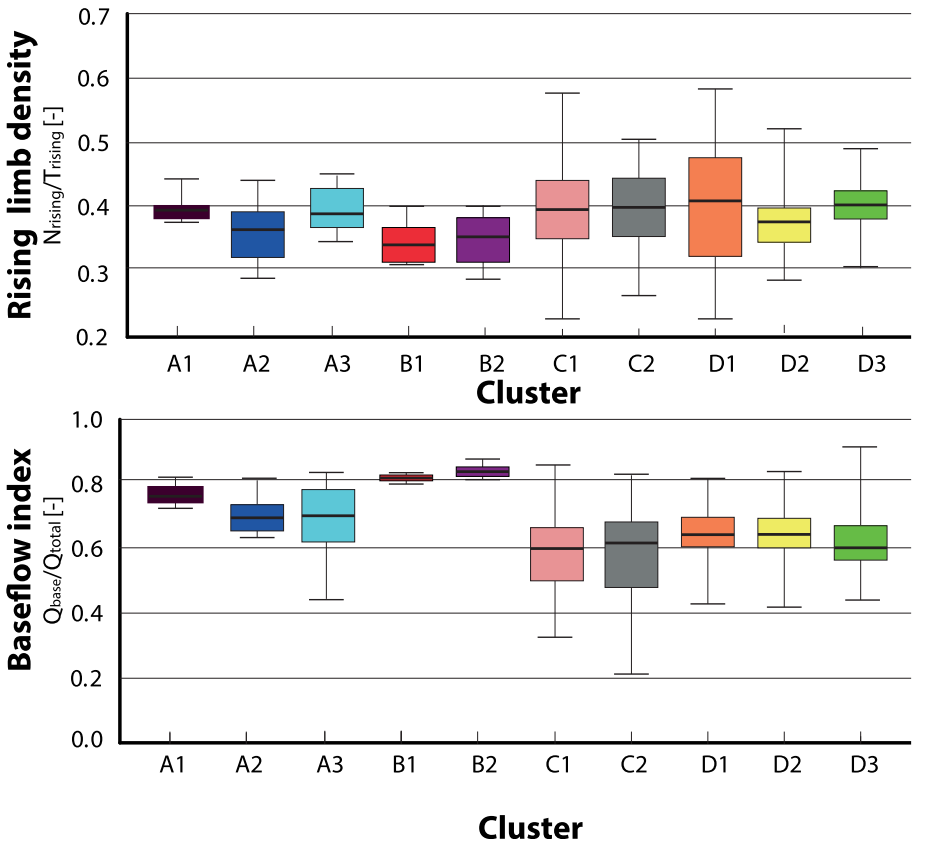

Figure 10. (top) The rising limb density and (bottom) base flow index values of the 10-catchment clusters displayed in whisker plots.

to very similar FDCs, as shown previously by *Yaeger et al.* [2012]. Where there is considerable variability within clusters (e.g., C1, C2), the variability is probably due to the role of the landscape properties, as well as event-scale responses that are not captured by the similarity framework but which would require extension of the model to include additional sources of variability in climate and/or catchment characteristics.

3.4.5. Flood Frequency Curve and the Flood Growth Curve

Figure 11 presents the growth curve (third row), the flood frequency curve (fourth row) and the timing of annual maximum flow (fifth row), using all available historical data, which in this case includes up to 54 years of daily flow data. Note that the flood growth curve is a plot of the ratio of annual maximum streamflow to the mean annual flood (linear scale) as a function of the Gumbel reduced variate. The flood frequency curve is the plot of the actual (nonnormalized) annual maximum streamflow (in this case, presented at a logarithmic scale) also as a function of the Gumbel reduced variate. Note that the analysis of floods here has been carried out based on daily flows only, which has obvious limitations for flood frequency analysis. Nevertheless, both signatures are valuable indicators of the variability of extreme (annual maximum) flows. The results show significant similarity and differences between and within the clusters, and once again an imprint of the seasonal water balance can be seen in both signatures. For example, the growth curves for A1 and B1 show remarkable Extreme Value Type I (EV-I or Gumbel)-like behavior (straight line), whereas the arid clusters, $(A3, C2)$, show more nonlinear, EV-II-like behavior, in line with the findings of *Farquharson et al.* [1992]. Catchments with high snowfall, $(B1,\ B2,\ f_s > 0.45)$, show very low within-cluster variability, whereas the arid catchments belonging to *A3* and *C2* show increasing within-cluster variability with increasing return period. Of the remaining clusters, the humid catchments belonging to D1, D2, and D3 show a common, compact (and linear) behavior up to a threshold value of return period, after which there is substantial within-cluster variability. This suggests a mix of flood producing processes (rainfall or snowmelt driven) and a change of process with increasing return period, partly contributed to by seasonality. Absolute flood values show considerable between-cluster variability mainly reflecting the wetness of

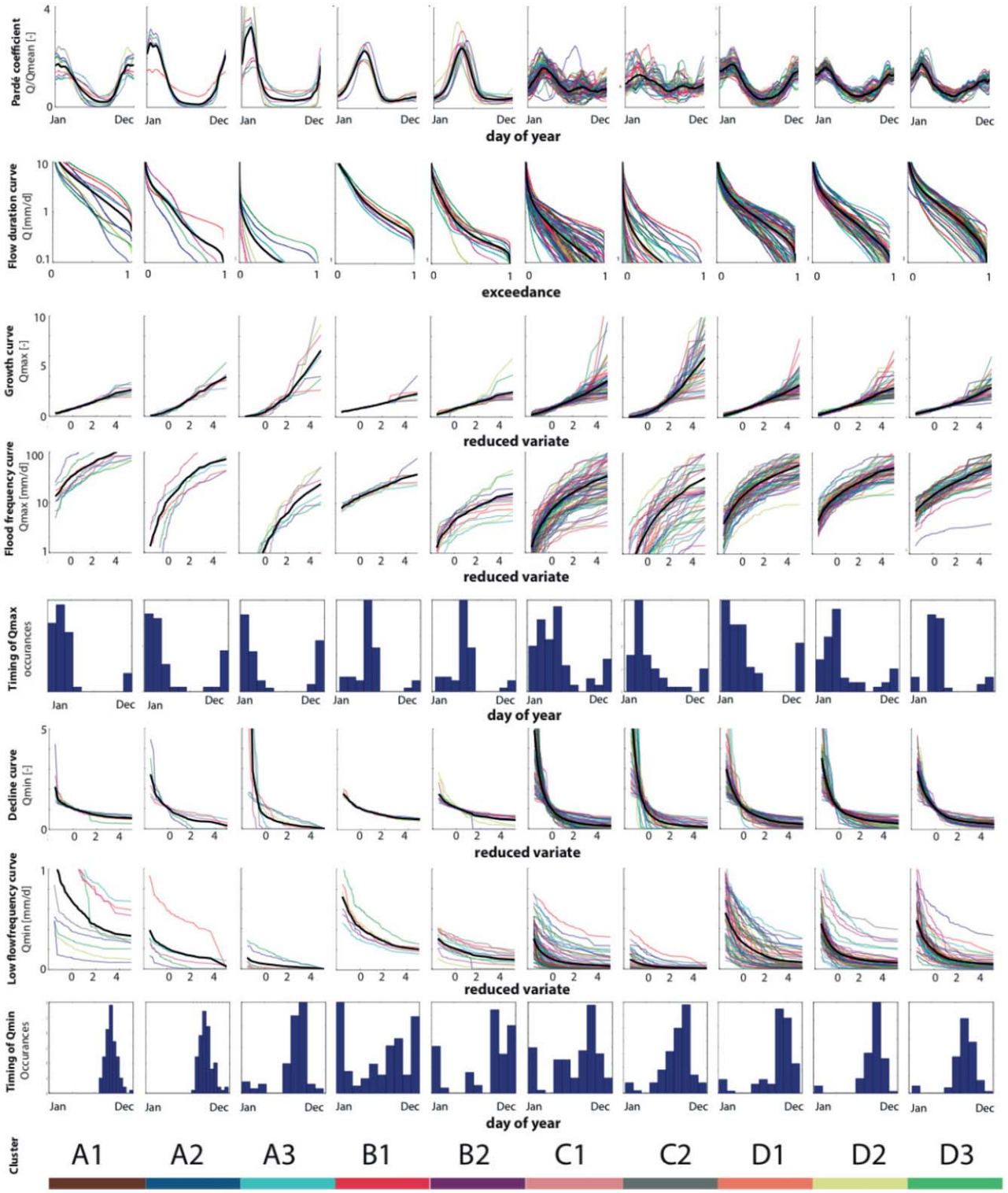

Figure 11. Overview of the various signature values of the 10-catchment clusters. Signatures included are (first row) the Pardé coefficients, (second row) the flow duration curve, (third row) the flood growth curve, (fourth row) the flood frequency curve, (fifth row) the timing of annual maximum flows, (sixth row) the decline curve, (seventh row) the low flow frequency curve, and (eight row) the timing of the low flow occurrences. The thin colored-lines display values of the individual catchments. The thicker black lines display the within-cluster average values.

the catchments (a function of aridity), and considerable within-cluster variability for catchments with a high aridity and low seasonal variability, i.e., $(C1, C2: AI > 0.90)$, but also for the more humid catchments D1, D2, and D3. Most clusters show strong seasonality in the timing of maximum flows, which is linked to the timing of maximum storage, although there is considerable variability between the clusters. Catchments in which storage variations are the smallest (C1, C2) also have the highest uncertainty in the timing of peak flows.

3.4.6. Low Flow Frequency Curve and Decline Curve

Figure 11 presents the decline curve (sixth row), the low flow frequency curve (seventh row), and the timing of the minimum flows (eighth row). The decline curve expresses the annual minimum discharge of 15 consecutive days, as a fraction of the mean annual minimum discharge, as a function of the Gumbel reduced variate. On the other hand, the low flow frequency curve expresses the minimum discharge of 15 consecutive days as a function of the Gumbel reduced variate. Both curves are constructed using all available historical data per catchment. Figure 11 indicates that generally the between-year variability of low flows increases with climatic aridity. Catchments with high winter precipitation $(A1, A2, A3: \delta_P^* < -0.3)$ and snowmelt influence $(B1, B2: f_s > 0.45)$ have a low between-year variability of low flows, as both catchment types experience recharge of soil water storage before the summer period begins. Arid and semiarid catchments with precipitation and evaporation in phase $(C1, C2: AI > 0.9, \delta_P^* > 0.0)$ fall dry during part of the year, because marginal soil water storage variations are unable to buffer dry periods. The timing of low flows also shows considerable variability between clusters, since seasonal climate determines the soil water storage patterns, which are largely in line with the timing of minimum flow.

4. Discussion of Results

4.1. On the Similarity of Seasonal Water Balance

The patterns displayed in Figure 7 indicate that the grouping procedure used in the study has produced coherent spatial clusters of similar seasonal water balances that satisfy the set criteria of minimum within-cluster variance and maximum between-cluster variance. Admittedly, the clustering presented here is based on seasonal water balance predictions by a conceptual model calibrated to observed streamflows. Without independent information on evaporation, soil moisture, and snow storage, the results are likely to include some degree of equifinality, i.e., there could be more or less evaporation (or storage) than is predicted by the model. Until more information is available, the clustering of catchments can be deemed as a hypothesis that remains to be tested.

The clusters of hydrologically similar basins are not only hydrologically coherent [e.g., *Kennard et al*., 2010; *Sawicz et al*., 2011; *Petersen et al*., 2012], but are also physiographically and climatically coherent. The spatial pattern of catchment clusters is largely overlapping with previous classification studies based on streamflow signatures [*Sawicz et al*., 2011; *Coopersmith et al*., 2012] or dominant process controls [*Ye et al*., 2012]. Compared to these studies, we exposed hydrological coherence at a wider range of time scales (daily to decadal), a wider range of states (low flows to floods), and a wider range of processes (water balance components). Clusters are characterized by the magnitudes of three climatic indices relating to aridity, precipitation timing, and snowiness. Compared to *Coopersmith et al*. [2012], the amount of similarity indices to distinguish between different classes is reduced, and now only depends on climatic variables. Our indices account for the role of snow. Snow is not explicitly included in the indices of *Coopersmith et al*. [2012] and *Petersen et al*. [2012].

In general, classes with more catchments naturally have larger within-class variability of hydrologic regimes. This larger range of variability can be due to the larger number of catchments within the cluster, but can also be due to the larger diversity of physiographic, anthropogenic, or climatic factors within a cluster. Attribution of the larger within-cluster variability requires further detailed study of individual clusters or regions. Similar to *Coopersmith et al*. [2012], these results may suggest that the seasonal water balance is primarily controlled by climate. However, as shown in Figure 8, the clusters also coincide very well with well-known ecosystem, soil, and vegetation classes. This not only lends credence to the grouping achieved on the basis of the seasonal water balance, but indicates a codependence of vegetation with seasonal water balance, i.e., the type of vegetation and its dynamics impact the seasonal water balance, but on the other hand the vegetation type and dynamics also reflect the water balance. The seasonal water balance thus provides

ecohydrological insights into the regional patterns of climate-soil-vegetation dynamics and helps to delineate regions with fundamentally different hydrologic regimes [*Rodriguez-Iturbe*, 2000]. This study also confirms previous results from ecological studies that have shown that it is not annual precipitation but seasonal precipitation and timing that govern vegetation types and functioning, and their geographic distribution [*Stephenson*, 1990; *Robinson et al*., 2012].

The seasonal water balances presented in Figure 6 also reveal differences in certain dominant features that drive or reflect the seasonality of the water balance. Snowmelt and snow storage, driven by snowiness of precipitation are the dominant features in clusters B1 and B2. Carry-over of soil moisture and groundwater storage, in response to a strong out-of-phase seasonality, is the dominant driver in clusters A1, A2, and A3. Surface soil moisture variations, likely driven by storm events, appear to be the main drivers of the seasonal water balance in clusters C1 and C2. Finally, vegetation phenology driven by seasonal variations of energy (and possibly soil moisture storage) is the main driver of seasonal water balance in clusters D2 and D3. These dominant processes are consistent with both the seasonal climate and the types of vegetation that are present: A1, B1, B2 (coniferous), A2 (coniferous forest and shrubs), B3 (shrubs), C1, C2 (short grass prairie and long grass prairie), D2, D3 (deciduous), and D1 (mixed deciduous/coniferous). The close association between the seasonal water balances, as reflected in these dominant features, and the types and functioning of the vegetation present, along with the patterns of seasonal variation of actual evaporation seen in Figure 6, bring attention to the different mechanisms that vegetation may have adopted to respond to and also reflect the seasonal water balance behavior. Examples of such adaptation include the carry-over of storage from wet to dry periods in clusters A1 and A2, and seasonal phenology changes in clusters D2 and D3.

Thus, in spite of the fact that the similarity framework used quantitative measures of similarity based on climate, it is still relying heavily on adaptation of the landscape, especially vegetation, to the climate. There is no guarantee that another place in the world with the same climate factors will evolve in the same way, in the presence of a different topography and geology (or parent material). To be universally applicable, the similarity framework must find a way to explicitly account for the role of landscape factors. A similarity framework based on a combination of climate and landscape characteristics is feasible in theory [e.g., *Yokoo and Sivapalan*, 2011], but suffers from the inability to specify the controlling landscape properties in an unambiguous manner for a large number of catchments. Evidence is emerging that model parameters relating to landscape properties are dependent upon climatic factors [*Milly*, 1994; *Troch et al*., 2013]. This codependence is an issue that requires focused research efforts in the future before we can complete the development of universal catchment classification schemes, and is beyond the scope of the present empirical study. The framework proposed here also suffers from the fact that local climate variations are not fully represented in the formulation, e.g., the bimodal rainfall patterns present in some southern states.

4.2. On the Link of Seasonal Water Balance to Other Streamflow Signatures

Now that the catchment grouping has revealed catchment clusters which exhibit strong similarities of seasonal water balance, including clear and unique features, how much of an imprint of the nature of seasonality is present in other signatures of streamflow variability? Addressing this question might help to highlight secondary controls, and generate a more holistic understanding of streamflow variability.

Results presented in Figure 9 clearly indicated that at the annual scale, the nature of seasonality introduces a distinct element to the Budyko curve, in the way the classes organize themselves. Out-of-phase seasonality and snowiness have the effect of reducing the annual evaporation (and increasing annual streamflow) compared to Budyko's predictions. Likewise, in-phase seasonality has the effect of increasing annual mean evaporation (and reducing annual mean streamflow).

On the other hand, while interannual variability of annual streamflow is mostly affected by aridity, there is also a significant contribution due to climate seasonality, especially in semiarid and arid basins with in-phase seasonality (e.g., C1 and C2). The effects of seasonality are also mediated by landscape factors, as reflected in the base flow index (BFI): higher BFI works together with strong seasonality to reduce interannual variability, as shown in the results of Figure 9. It is to be noted that mountainous catchments (clusters B1, B2) have a higher BFI than flatter catchments (clusters C1 and C2). This may be an artifact of the higher snowmelt component.

Results presented in Figure 11 indicate that the remaining signatures show a combination of the effects of seasonality and landscape properties. The timing of flood peaks and low flows is strongly affected by

seasonality, which then impacts on the shapes of both flood frequency curves and low flow frequency curves. Aridity impacts the slope of the FFC (growth curves are more nonlinear with increasing aridity), clusters that include out-of-phase seasonality and snowiness show strong within-cluster compactness. The presence of in-phase seasonality and storminess contributes to significant within-cluster variability.

The patterns of streamflow signatures, and their link to climatic indices, can potentially be used to predict streamflow signatures when no streamflow measurements are available. Additionally, it may help to identify or interpret changes of hydrological behavior in response to climate change. *Coopersmith et al*. [2014] used the similarity indices of *Coopersmith et al*. [2012] to classify temporal shifts in seasonal streamflow. Our similarity indices can be used in a similar fashion, but now to describe hydrological shifts for a wider range of time scales, conditions, and processes.

Vegetation [*Rodriguez-Iturbe*, 2000] and the composition of the landscape [*Savenije*, 2010] in combination with geology [*Winter*, 2001] are clearly significant controls on observed hydrological behavior. At long time scales and large space scales some of these factors have been implicitly factored into the grouping of catchments through their imprint in the observed seasonal water balances. An example is BFI, which is largely determined by landscape characteristics and in some cases by snowiness, as in the case of mountainous catchments in the western U.S. [*Santhi et al*., 2008]: clearly, it is of major importance under low flow conditions, but has been found to also impact the shape of the flood growth curve [*Guo et al*., 2014]. On the other hand, at small time and space scales, the landscape characteristics that matter are those that determine the responsiveness of a catchment to precipitation inputs. Including such landscape characteristics in the similarity framework will very likely improve the prediction of these signatures. Until truly universal similarity frameworks are developed that capture streamflow variability at a range of time scales, streamflow observations and signatures of streamflow variability remain the best objective and holistic metrics of catchment similarity: this has been the rationale of previous catchment classification studies [*Wagener et al*., 2007; *Kennard et al*., 2010; *Sawicz et al*., 2011; *Coopersmith et al*., 2012].

5. Conclusions

In this study, we have used a conceptual rainfall-runoff model to compute the seasonal water balance behavior of over 300 catchments across the continental U.S., and to bring out interesting coherent spatial patterns. Using the computed seasonal water balances, we grouped catchments into 10 coherent clusters having similar behavior, satisfying the criteria of minimum variance within clusters and maximum variance between clusters. We developed a similarity framework based on three climate indices alone, i.e., climatic aridity, timing of seasonal precipitation, and a temperature-based measure of snowiness, that provide a backdrop to, and explanations for, the observed similarities and differences. While the clustering of catchments is based on the seasonal water balance, and has a strong relationship to regional patterns of the three climate indices, both of these spatial patterns have been shown to map on to well-known regional ecosystem, soil, and vegetation classes. These results suggest that the dominant soil orders and vegetation types are not only climate dependent, but also that vegetation and soils both contribute to and are a reflection of the seasonal water balance regime. The dominant processes attributed to each of the catchment clusters can thus be deemed as different mechanisms through which vegetation and soils adapt to and modify the seasonal water balance in each case. A major element of the adaptation of the landscape with the seasonal climate is manifested differently in the processes or seasonal water balance behavior in different places: carry-over of soil moisture in California, snow storage and melt in the Rocky Mountains, and phenology in north-east U.S.

The paper has also demonstrated that the seasonal water balance patterns provide a useful backdrop to the streamflow variability over a wide range of time scales (daily to decadal) and states (low flow to floods). On seasonal to longer (mean annual and interannual variability) time scales, streamflow variability either directly, or indirectly through adaptation of landscape features with climate, reflects the nature of seasonal water balance. On shorter time scales, streamflow variability is a result of the interaction of climate directly with the landscape, including topography, vegetation and soil. Until these landscape factors are included, the similarity framework will remain incomplete and not universally applicable. All the signatures of streamflow variability considered here are outward manifestations of both short-term hydrologic responses and

long-term adaptation of the landscape with climate, and therefore reflect as well as impact patterns of seasonal water balances, which are normally unobserved internal dynamics of catchments.

Acknowledgments
We are grateful to Matej Durcik of SAHRA (University of Arizona) for providing the version of the MOPEX data set used in this study. We thank Sheng Ye for providing part of the data used in the study, Shervan Gharari for valuable inputs to the modeling, and Mary Yaeger for sharing her insights on an earlier draft of this paper. WRB is grateful for the Justus and Louise van Effen Research grant, which enabled him to spend a few months at the University of Illinois, where much of this work was completed. We thank the editor and two anonymous reviewers for their constructive comments, which helped to clarify several important points in the manuscript.

References

Andréassian, V., J. Lerat, N. Le Moine, and C. Perrin (2012), Neighbors: Nature's own hydrological models, *J. Hydrol.*, *414*, 49–58.
Arnold, J. G., P. M. Allen, R. Muttiah, and G. Bernhardt (1995), Automated base flow separation and recession analysis techniques, *Ground Water*, *33*(6), 1010–1018.
Atkinson, S. E., R. A. Woods and M. Sivapalan (2002), Climate and landscape controls on water balance model complexity over changing timescales, *Water Resour. Res.*, *38*(12), 1314, doi:10.1029/2002WR001487.
Bailey, R. G. (2009), *Ecosystem Geography: From Ecoregions to Sites*, 2nd ed., 251 pp., Springer, N. Y.
Beck, H. E., A. I. J. M. van Dijk, D. G. Miralles, R. A. M. de Jeu, L. A. Bruijnzeel, T. R. McVicar, and J. Schellekens (2013), Global patterns in base flow index and recession based on streamflow observations from 3394 catchments, *Water Resour. Res.*, *49*, 7843–7863, doi:10.1002/2013WR013918.
Berghuijs, W. R., R. A. Woods, and M. Hrachowitz (2014), A precipitation shift from snow towards rain leads to a decrease in streamflow, *Nat. Clim. Change*, *4*, 583–586, doi:10.1038/nclimate2246.
Beven, K. J. (2000), Uniqueness of place and process representations in hydrological modelling, *Hydrol. Earth Syst. Sci.*, *4*(2), 203–213.
Blöschl, G., M. Sivapalan, T. Wagener, A. Viglione and H. H. G. Savenije (Eds.) (2013), *Runoff Prediction in Ungauged Basins: Synthesis Across Processes, Places and Scales*, 500 pp., Cambridge Univ. Press, Cambridge, U. K.
Breinlinger, R. (1996), Hydrogeographische Raumgliederung der Schweiz und ihre Bedeutung für die Hydrologie, PhD dissertation, Geogr. Inst. of the Univ. of Berne, Bern, Switzerland.
Budyko, M. I. (1974), *Climate and Life*, Academic, N. Y.
Coopersmith, E., M. A. Yaeger, S. Ye, L. Cheng, and M. Sivapalan (2012), Exploring the physical controls of regional patterns of flow duration curves—Part 3: A catchment classification system based on regime curve indicators, *Hydrol. Earth Syst. Sci.*, *16*, 4467–4482.
Coopersmith, E. J., B. S. Minsker, and M. Sivapalan (2014), Patterns of regional hydroclimatic shifts: An analysis of changing hydrologic regimes, *Water Resour. Res.*, *50*, 1960–1983, doi:10.1002/2012WR013320.
Dooge, J. C. I. (1986), Looking for hydrology laws, *Water Resour. Res.*, *22*(9), 465–585.
Dooge, J. C. I. (1992), Hydrologic models and climate change, *J. Geophys. Res.*, *97*(D3), 2677–2686.
Duan, Q., et al. (2006), Model Parameter Estimation Experiment (MOPEX): An overview of science strategy and major results from the second and third workshops, *J. Hydrol.*, *320*(1-2), 3–17.
Eckhardt, K. (2008), A comparison of baseflow indices, which were calculated with seven different baseflow separation methods, *J. Hydrol.*, *352*(1), 168–173.
Eder, G., M. Sivapalan, and H. P. Nachtnebel (2003), Modelling water balances in an Alpine catchment through exploitation of emergent properties over changing time scales, *Hydrol. Processes*, *17*(11), 2125–2149.
Falkenmark, M., and T. Chapman (1989), *Comparative Hydrology: An Ecological Approach to Land and Water Resources*, The UNESCO Press, Paris, France.
Farmer, D., M. Sivapalan, and C. Jothityangkoon (2003), Climate, soil, and vegetation controls upon the variability of water balance in temperate and semiarid landscapes: Downward approach to water balance analysis, *Water Resour. Res.*, *39*(2), 1035, doi:10.1029/2001WR000328.
Farquharson, F. A. K., J. R. Meigh, and J. V. Sutcliffe (1992), Regional flood frequency analysis in arid and semi-arid areas, *J. Hydrol.*, *138*(3), 487–501.
Fenicia, F., H. H. G. Savenije, P. Matgen and L. Pfister (2008), Understanding catchment behavior through stepwise model concept improvement, *Water Resour. Res.*, *44*, W01402, doi:10.1029/2006WR005563.
Gerrits, A. M. J., H. H. G. Savenije, E. J. M. Veling and L. Pfister (2009), Analytical derivation of the *Budyko* curve based on rainfall characteristics and a simple evaporation model, *Water Resour. Res.*, *45*, W04403, doi:10.1029/2008WR007308.
Güntner, A., J. Stuck, S. Werth, P. Döll, K. Verzano, and B. Merz (2007), A global analysis of temporal and spatial variations in continental water storage, *Water Resour. Res.*, *43*, W05416, doi:10.1029/2006WR005247.
Guo, J., H.-Y. Li, L. R. Leung, S. Guo, P. Liu, and M. Sivapalan (2014), Links between flood frequency and annual water balance behaviors: A basis for similarity and regionalization, *Water Resour. Res.*, *50*, 937–953, doi:10.1002/2013WR014374.
Haines, A. T., B. L. Finlayson, and T. A. McMahon (1988), A global classification of river regimes, *Appl. Geogr.*, *8*(4), 255–272.
Hannah, D. M., S. R. Kansakar, A. J. Gerrard, and G. Rees (2005), Flow regimes of Himalayan rivers of Nepal: Nature and spatial patterns, *J. Hydrol.*, *308*(1), 18–32.
Harris, N. M., A. M. Gurnell, D. M. Hannah, and G. E. Petts (2000), Classification of river regimes: A context for hydro-ecology, *Hydrol. Processes*, *14*(16-17), 2831–2848.
Hickel, K., and L. Zhang (2006), Estimating the impact of rainfall seasonality on mean annual water balance using a top-down approach, *J. Hydrol.*, *331*(3), 409–424.
Jakeman, A. J., and G. M. Hornberger (1993), How much complexity is warranted in a rainfall-runoff model?, *Water Resour. Res.*, *29*(8), 2637–2649.
Kennard, M. J., B. J. Pusey, J. D.Olden, S. J. MacKay, J. L. Stein, and N. Marsh (2010), Classification of natural flow regimes in Australia to support environmental flow management, *Freshwater Biol.*, *55*(1), 171–193.
Klemeš, V. (1988), A hydrological perspective, *J. Hydrol.*, *100*(1), 3–28.
Köppen, W. (1936), Handbuch der Climatologie, Köppen-Geiger, Gebrüder Borntraeger, Berlin, Germany.
Kroll, C., J. Luz, B. Allen, and R. M. Vogel (2004), Developing a watershed characteristics database to improve low streamflow prediction, *J. Hydrol. Eng.*, *9*(2), 116–125.
Laizé, C. L., and D. M. Hannah (2010), Modification of climate–river flow associations by basin properties, *J. Hydrol.*, *389*(1), 186–204.
Li, D., M. Pan, Z. Cong, L. Zhang, and E. F. Wood (2013), Vegetation control on water and energy balance within the Budyko framework, *Water Resour. Res.*, *49*, 969–976, doi:10.1002/wrcr.20107.
Lo, M. H., J. S. Famiglietti, P. F. Yeh, and T. H. Syed (2010), Improving parameter estimation and water table depth simulation in a land surface model using GRACE water storage and estimated base flow data, *Water Resour. Res.*, *46*, W05517, doi:10.1029/2009WR007855.
McDonnell, J. J., et al. (2007), Moving beyond heterogeneity and process complexity: A new vision for watershed hydrology, *Water Resour. Res.*, *43*, W07301, doi:10.1029/2006WR005467.

McMahon, T. A., et al. (2013), Prediction of annual runoff in ungauged basins, in *Runoff Prediction in Ungauged Basins: Synthesis Across Processes, Places and Scales*, edited by G. Blöschl et al., pp. 70–101, Cambridge Univ. Press, Cambridge, U. K.
Milly, P. C. D. (1994), Climate, soil water storage, and the average annual water balance, *Water Resour. Res.*, *30*(7), 2143–2156.
Milly, P. C. D., and K. A. Dunne (2002), Macroscale water fluxes: 2. Water and energy supply control of their inter-annual variability, *Water Resour. Res.*, *38*(10), 1206, doi:10.1029/2001WR000760.
Moriasi, D. N., J. G. Arnold, M. W. Van Liew, R. L. Bingner, R. D. Harmel, and T. L. Veith (2007), Model evaluation guidelines for systematic quantification of accuracy in watershed simulations, *Trans. ASABE*, *50*(3), 885–900.
Nash, J., and J. V. Sutcliffe (1970), River flow forecasting through conceptual models part I—A discussion of principles, *J. Hydrol.*, *10*(3), 282–290.
Pardé, M. (1933), *Fleuves et Rivières*, vol. 1, Armand Colin, Paris.
Peel, M. C., B. L. Finlayson, and T. A. McMahon (2007), Updated world map of the Koppen-Geiger climate classification, *Hydrol. Earth Syst. Sci.*, *11*, 1633–1644.
Petersen, T., N. Devineni, and A. Sankarasubramanian (2012), Seasonality of monthly runoff over the continental United States: Causality and relations to mean annual and mean monthly distributions of moisture and energy, *J. Hydrol.*, *468–469*, 139–150.
Pike, J. G. (1964), The estimation of annual run-off from meteorological data in a tropical climate, *J. Hydrol.*, *2*(2), 116–123.
Potter, N. J., L. Zhang, P. C. D. Milly, T. A. McMahon, and A. J. Jakeman (2005), Effects of rainfall seasonality and soil moisture capacity on mean annual water balance for Australian catchments, *Water Resour. Res.*, *41*, W06007, doi:10.1029/2004WR003697.
Robinson, T. M., K. J. La Pierre, M. A. Vadeboncoeur, K. M. Byrne, M. L. Thomey, and S. E. Colby (2012), Seasonal, not annual precipitation drives community productivity across ecosystems, *Oikos*, *122*, 727–738, doi:10.1111/j.1600-0706.2012.20655.x.
Rodriguez-Iturbe, I. (2000), Ecohydrology: A hydrologic perspective of climate-soil-vegetation dynamics, *Water Resour. Res.*, *36*(1), 3–9.
Santhi, C., P. M. Allen, R. S. Muttiah, J. G. Arnold, and P. Tuppad (2008), Regional estimation of base flow for the conterminous United States by hydrologic landscape regions, *J. Hydrol.*, *351*(1), 139–153.
Savenije, H. H. G. (2001), Equifinality, a blessing in disguise?, *Hydrol. Processes*, *15*(14), 2835–2838.
Savenije, H. H. G. (2010), HESS opinions: Topography driven conceptual modelling (FLEX-Topo), *Hydrol. Earth Syst. Sci.*, *14*(12), 2681–2692.
Sawicz, K., T. Wagener, M. Sivapalan, P. A. Troch, and G. Carrillo (2011), Catchment classification: Empirical analysis of hydrologic similarity based on catchment function in the eastern USA, *Hydrol. Earth Syst. Sci.*, *15*, 2895–2911.
Schaake, J., S. Cong, and Q. Duan (2006), The US MOPEX data set, *IAHS Publ.*, *307*, 9–28.
Shamir, E., B. Imam, E. Morin, H. V. Gupta, and S. Sorooshian (2005), The role of hydrograph indices in parameter estimation of rainfall–runoff models, *Hydrol. Processes*, *19*(11), 2187–2207.
Sivapalan, M. (2003), Process complexity at hillslope scale, process simplicity at the watershed scale: Is there a connection?, *Hydrol. Processes*, *17*, 1037–1041.
Sivapalan, M. (2005), Pattern, process and function: Elements of a unified theory of hydrology at the catchment scale, in *Encyclopedia of Hydrological Sciences*, chap. 12, edited by M. J. Anderson, John Wiley, Chichester, U. K., 193–213.
Stephenson, N. L. (1990), Climatic control of vegetation distribution: The role of the water balance, *Am. Nat.*, *135*, 649–670.
Thompson, S. E., C. J. Harman, A. G. Konings, M. Sivapalan, and P. A. Troch (2011), Comparative hydrology across Ameriflux sites: The variable roles of climate, vegetation and groundwater, *Water Resour. Res.*, *47*, W00J07, doi:10.1029/2010WR009797.
Thornthwaite, C. W., and J. R. Mather (1955), *The Water Balance*, vol. 8, Drexel Inst. of Technol., Centerton, N. J.
Troch, P. A., G. F. Martinez, V. R. N. Pauwels, M. Durcik, M. Sivapalan, C. J. Harman, P. D. Brooks, H. V. Gupta, and T. E. Huxman (2009), Climate and vegetation water-use efficiency at catchment scales, *Hydrol. Processes*, *23*, 2409–2414, doi:10.1002/hyp.7358.
Troch, P. A., G. Carrillo, M. Sivapalan, T. Wagener, and K. Sawicz (2013), Climate-vegetation-soil interactions and long-term hydrologic partitioning: Signatures of catchment co-evolution, *Hydrol. Earth Syst. Sci.*, *17*, 2209–2217, doi:10.5194/hess-17–2209-2013.
U.S. Soil Taxonomy (2014), Soil regions of the United States, Map, Encyclopedia Britannica, London. [Available at http://www.britannica.com/EBchecked/media/19522, last accessed 28 Mar. 2014.].
Vogel, R. M., and N. M. Fennessey (1995), Flow duration curves II, *Water Resour. Bull.*, *31*, 1029–1039.
Vogel, R. M., and C. N. Kroll (1992), Regional geohydrologic-geomorphic relationships for the estimation of low-flow statistics, *Water Resour. Res.*, *28*(9), 2451–2458.
Vrugt, J. A., H. V. Gupta, W. Bouten, and S. Sorooshian (2003), A Shuffled Complex Evolution Metropolis algorithm for optimization and uncertainty assessment of hydrologic model parameters, *Water Resour. Res.*, *39*(8), 1201, doi:10.1029/2002WR001642.
Wagener, T., M. Sivapalan, P. A. Troch, and R. A. Woods (2007), Catchment classification and hydrologic similarity, *Geogr. Compass*, *1*(4), 901–931.
Weingartner, R., and H. Aschwanden (1992), Discharge regime–the basis for the estimation of average flows, in *Hydrological Atlas of Switzerland, Map 5.2,* Swiss Federal Office for the Environment, Bern, Switzerland.
Willmott, C. J., C. M. Rowe, and Y. Mintz (1985), Climatology of the terrestrial seasonal water cycle, *J. Climatol.*, *5*(6), 589–606.
Winter, T. C. (2001), The concept of hydrologic landscapes, *J. Am. Water Resour. Assoc.*, *37*, 335–349.
Woods, R. A. (2003), The relative roles of climate, soil, vegetation and topography in determining seasonal and long-term catchment dynamics, *Adv. Water Resour.*, *26*(3), 295–309.
Woods, R. A. (2009), Analytical model of seasonal climate impacts on snow hydrology: Continuous snowpacks, *Adv. Water Resour.*, *32*(10), 1465–1481.
Wundt, W. (1953), *Gewässerkunde*, Springer, Berlin, Germany.
Yaeger, M., E. Coopersmith, S. Ye, L. Cheng, A. Viglione, and M. Sivapalan (2012), Exploring the physical controls of regional patterns of flow duration curves-Part 4: A synthesis of empirical analysis, process modeling and catchment classification, *Hydrol. Earth Syst. Sci.*, *16*, 4483–4498.
Ye, S., M. Yaeger, E. Coopersmith, L. Cheng, and M. Sivapalan (2012), Exploring the physical controls of regional patterns of flow duration curves–Part 2: Role of seasonality, the regime curve, and associated process controls, *Hydrol. Earth Syst. Sci.*, *16*(11), 4447–4465.
Yokoo, Y., and M. Sivapalan (2011), Towards reconstruction of the flow duration curve: Development of a conceptual framework with a physical basis, *Hydrol. Earth Syst. Sci.*, *15*(9), 2805–2819.
Yokoo, Y., M. Sivapalan, and T. Oki (2008), Investigating the roles of climate seasonality and landscape characteristics on mean annual and monthly water balances, *J. Hydrol.*, *357*(3), 255–269.
Zhang, L., W. R. Dawes, and G. R. Walker (2001), Response of mean annual evapotranspiration to vegetation changes at catchment scale, *Water Resour. Res.*, *37*(3), 701–708.